Fig. 2. Neuroprotective effect of HGF on facial (a and b) and hypoglossal (c and d) motoneurons in G93A mice. (a and c) Photomicrographs of representative Nissl-stained sections of the facial (a) and hypoglossal (c) nuclei of WT, HGF-Tg, G93A, and G93A/HGF mice at 8 months of age are shown. Scale bars = 50 μm. (b and d) Quantification of the mean numbers of surviving Nissl-stained neuronal cells with a clear nucleolus in the facial (b) and hypoglossal (d) nuclei of 8-month-old mice of each group. Motoneuron survival is expressed as the neuronal cell count on every fifth section of 16 sections. Data represent the mean ± S.E. (n = 4 for each group). **P < 0.01 compared with WT and G93A/HGF mice.

(a microglia marker; Imai et al., 1996) and GFAP (an astrocyte marker). As shown in Fig. 3a, microglia densely accumulated in the facial nuclei of G93A mice at 8 months of age, while the number of microglia was lower in the facial nuclei of WT and HGF-Tg mice. The mean intensity of Iba1-IR in the facial nuclei of G93A mice increased 3.7-fold over the WT signal. In contrast, the mean intensity of Iba1-IR in the facial nuclei of G93A/HGF mice decreased to 59% of that found in G93A mice. Similar results were obtained for the hypoglossal nuclei (Fig. 3a).

Immunofluorescence analyses showed that a large number of hypertrophic astrocytes (i.e., exhibiting astrocytosis) were evident in the facial and hypoglossal nuclei of the G93A mice, while the number of astrocytes was low in the nuclei of both WT and HGF-Tg mice. Consistent with the reduction of Iba1-IR and GFAP-IR, the numbers of Iba1-positive and GFAP-positive cells were lower in G93A/HGF mice compared with G93A mice (data not shown). These results demonstrate that HGF is capable of suppressing both microgliosis (accumulation of activated microglia) and astrocytosis in the facial and hypoglossal nuclei of G93A mice.

3.5. HGF suppresses active caspase-1 and monocyte chemoattractant protein (MCP)-1 in facial and hypoglossal nuclei of G93A mice

The mechanisms by which HGF suppresses gliosis in the facial and hypoglossal nuclei of G93A mice were examined. The mRNA expression of monocyte chemoattractant protein (MCP)-1 is critical for recruitment of inflammatory cells of the monocytic lineage after inflammation or injury to the central nervous system (Berman et al., 1996). Compared with non-neurological disease controls, MCP-1 is markedly increased in the spinal cords of ALS patients and in transgenic mice overexpressing SOD1^{G37R} (G37R mice, a model of ALS) (Henkel et al., 2004, 2006; Baron et al., 2005). Intrathecal treatment with cyclosporin, which is thought to reduce MCP-1 levels, prolongs survival of late stage G93A mice (Keep et al., 2001). Therefore, HGF modulation of MCP-1 levels in the facial and hypoglossal nuclei of 8-month-old G93A mice was examined using immunohistochemistry. MCP-1-IR primarily localized to astrocyte-like cells in the facial nuclei of G93A mice. Double-fluorescence immunostaining revealed that MCP-1-IR with strong immunoreactivity co-localized well
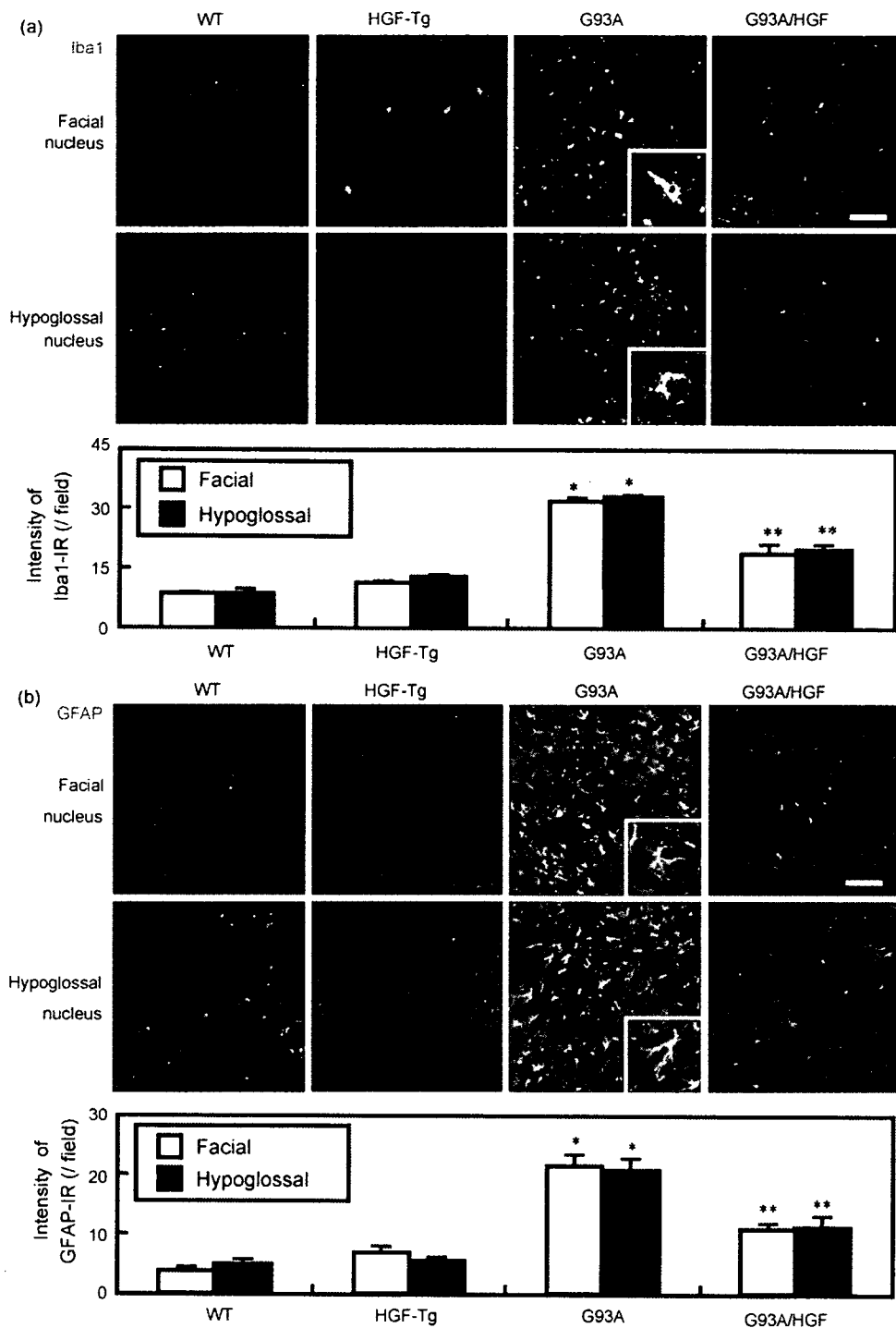
Fig. 3. Suppression of gliosis in the facial and hypoglossal nuclei of G93A/HGF mice. (a) Suppression of microglial accumulation in G93A/HGF mice. Immunofluorescence analysis for Iba1 (a marker for microglia) in the facial and hypoglossal nuclei of WT, HGF-Tg, G93A and G93A/HGF mice at 8 months of age. Scale bar = 100 μm. The intensity of Iba1-IR is shown in the facial (open column) and hypoglossal (closed column) nuclei. Data represent the mean ± S.E. (n = 4 for each group). *P < 0.05 vs. WT mice and **P < 0.05 vs. G93A mice. (b) Suppression of astrocytosis in G93A/HGF mice. Immunofluorescence analysis for GFAP (a marker for astrocyte) in the facial and hypoglossal nuclei of WT, HGF-Tg, G93A and G93A/HGF mice at 8 months of age. Scale bar = 100 μm. The intensity of GFAP-IR is shown in the facial (open column) and hypoglossal (closed column) nuclei. Data represent the mean ± S.E. (n = 4 for each group). *P < 0.05 vs. WT mice and **P < 0.05 vs. G93A mice.

with GFAP, indicating that MCP-1-IR is predominantly induced in reactive astrocytes (Fig. 4a, upper left panel). While double-fluorescence immunostaining of MCP-1 and tubulinβIII showed that weakly immunostained MCP-1-IR

cells in G93A mice were motoneurons, the signal was below the detection limit in the facial nuclei of WT mice (Fig. 4a, upper middle panel). In contrast with G93A mice, G93A/HGF mice showed much lower levels of MCP-1-IR in the facial nuclei
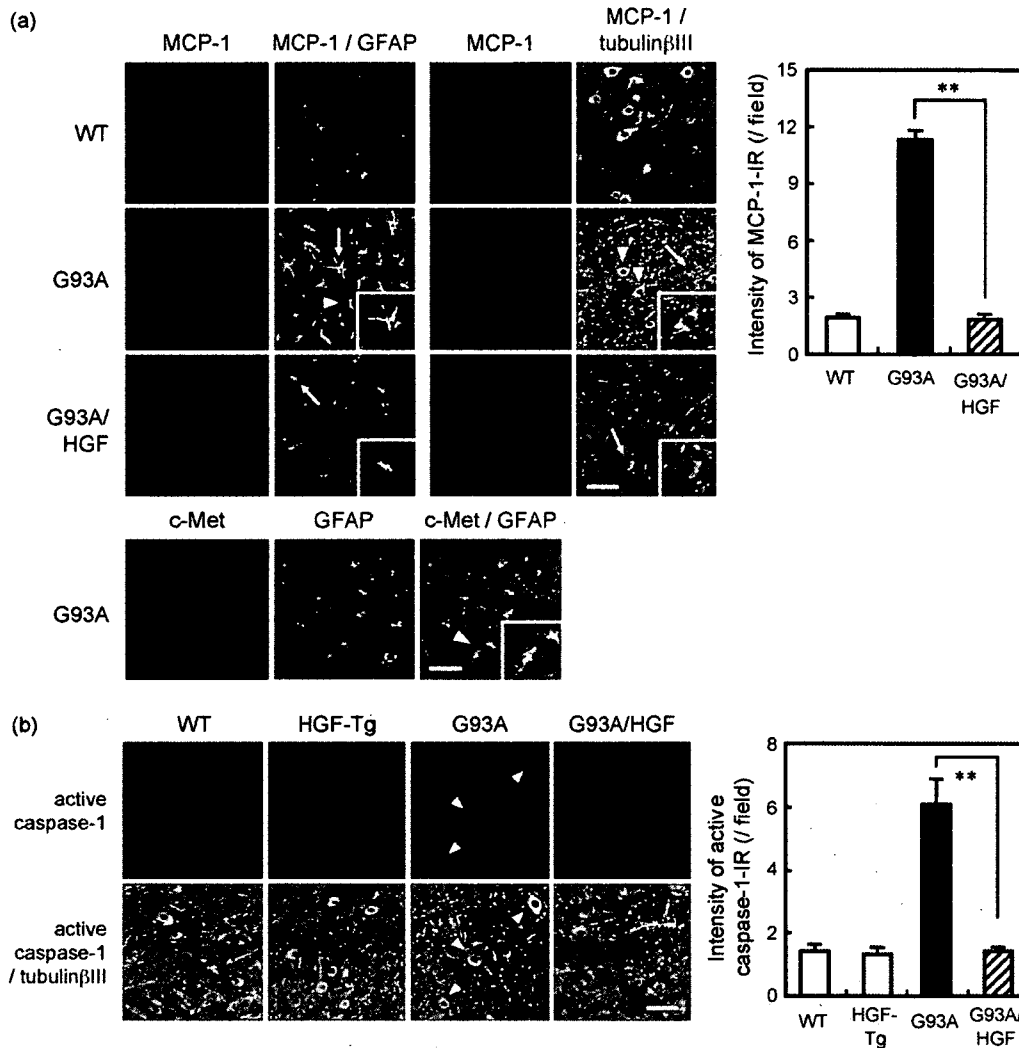
Fig. 4. Inhibitory mechanisms of HGF on gliosis in the facial nucleus of G93A mice. (a) Suppression of MCP-1 induction in G93A/HGF mice. Upper left panel, double immunofluorescence analysis of MCP-1 (red) and GFAP (green) or tubulinβIII (green) in the facial nucleus of WT, G93A and G93A/HGF mice at 8 months of age. Scale bars = 50 μm. Arrowheads indicate MCP-1-positive cells lacking GFAP-IR or double labeled with tubulinβIII-IR. A high-magnification view of the area indicated by the arrow is also shown. Lower left panel, double immunofluorescence analysis of c-Met (red) and GFAP (green) in the facial nucleus of G93A mice. A high-magnification view of the area indicated by the arrows is also boxed in each photograph. c-Met immunoreactivity was undetectable in reactive astrocytes of the facial nucleus of G93A mice. Upper right panel, the intensity of MCP-1-IR is shown in the facial nucleus of WT, G93A and G93A/HGF mice. Data represent the mean ± S.E. (n = 4 for each group). **P < 0.01 vs. G93A mice. (b) Suppression of caspase-1 activation in the facial nucleus of G93A/HGF mice. Left panel, double-immunofluorescence analysis of active caspase-1 (red) and tubulinβIII (green) in the facial nucleus of WT, HGF-Tg, G93A and G93A/HGF mice at 6 months of age. Active caspase-1-positive neurons are indicated by arrowheads. Right panel, the intensity of active caspase-1-IR is shown in the facial nucleus of WT, G93A and G93A/HGF mice. Data represent the mean ± S.E. (n = 4 for each group). **P < 0.01 vs. G93A mice.

(Fig. 4a, upper left and middle panels). The mean intensity of MCP-1-IR in the facial nuclei of G93A mice increased 5.8-fold relative to WT mice. Meanwhile, the mean intensity of MCP-1-IR in the facial nucleus of G93A/HGF mice was decreased, and was similar to the level observed in WT mice (Fig. 4a, upper right panel). Similar results were obtained for the hypoglossal nuclei of WT mice, G93A and G93A/HGF mice (data not shown).

How could MCP-1 induction in G93A mice be attenuated by HGF? Interleukin (IL)-1ß has been postulated to play a role in the induction of MCP-1 and astrocytosis in vivo (Giulian et al., 1988; Herx and Yong, 2001) and in vitro (John et al., 2004). IL-1ß is generated by proteolytic cleavage of pro-IL-1ß by IL-1ß-converting enzyme (ICE)/caspase-1 activation (Thornberry et al., 1992). Therefore, the effect of HGF on caspase-1

activation, which is abundant long before neuronal death and/or phenotypic onset (Pasinelli et al., 2000), mediation of disease processes from the early stage of the disease, was examined. Active caspase-1-IR was detectable in the facial motoneurons of G93A mice at 6 months of age (during the middle stage of the disease when motoneuronal death is not evident), but the immunofluorescent signal was undetectable in WT and HGF-Tg mice (Fig. 4b). G93A/HGF mice showed much lower levels of active caspase-1-IR in the facial motoneurons (Fig. 4b, left panel). The mean intensity of active caspase-1-IR in the facial nucleus of G93A mice increased significantly to 4.2-fold higher than in WT mice. Meanwhile, the mean intensity of caspase-1-IR in the facial nucleus of G93A/HGF mice was decreased, and was at almost the same level as in WT mice (Fig. 4b, right

panel). Similar results were obtained for the hypoglossal motoneurons (data not shown). Suppression of active caspase-1 induction by HGF might help reduce IL-1ß levels in motoneurons which, in turn, suppresses MCP-1 induction. This scenario explains the suppressive effect of HGF on gliosis, despite the observation that c-Met-IR was below the detection limit in astrocytes (Fig. 4a, lower panel) and microglia (data not shown) at the developmental stage examined.

3.6. HGF induces XIAP and attenuates pro-apoptotic protein activation in facial and hypoglossal motoneurons of G93A mice

The mechanism of the HGF neuroprotective effect on facial and hypoglossal motoneurons was examined using immuno-

histochemistry. Previous studies have demonstrated that caspases are activated in spinal motoneurons of a transgenic mouse model of ALS at various stages throughout the clinical course, and that caspase-mediated apoptosis is a mechanism of motoneuronal degeneration in ALS (Pasinelli et al., 2000; Li et al., 2000; Guegan et al., 2001; Inoue et al., 2003). Therefore, the effect of HGF on the activation of caspases-3 and -9 was examined. Active caspase-3-IR and caspase-9-IR were induced in facial motoneurons of G93A mice at 6 months of age, while the signal was not detected in the nuclei of WT or HGF-Tg mice (Fig. 5a and b). However, G93A/HGF mice showed much lower levels of active caspase-3-IR and caspase-9-IR in facial motoneurons (Fig. 5a and b, left panel). The mean intensities of active caspase-3-IR and caspase-9-IR in the facial nuclei of G93A mice increased significantly (5.6- and 6.4-fold,
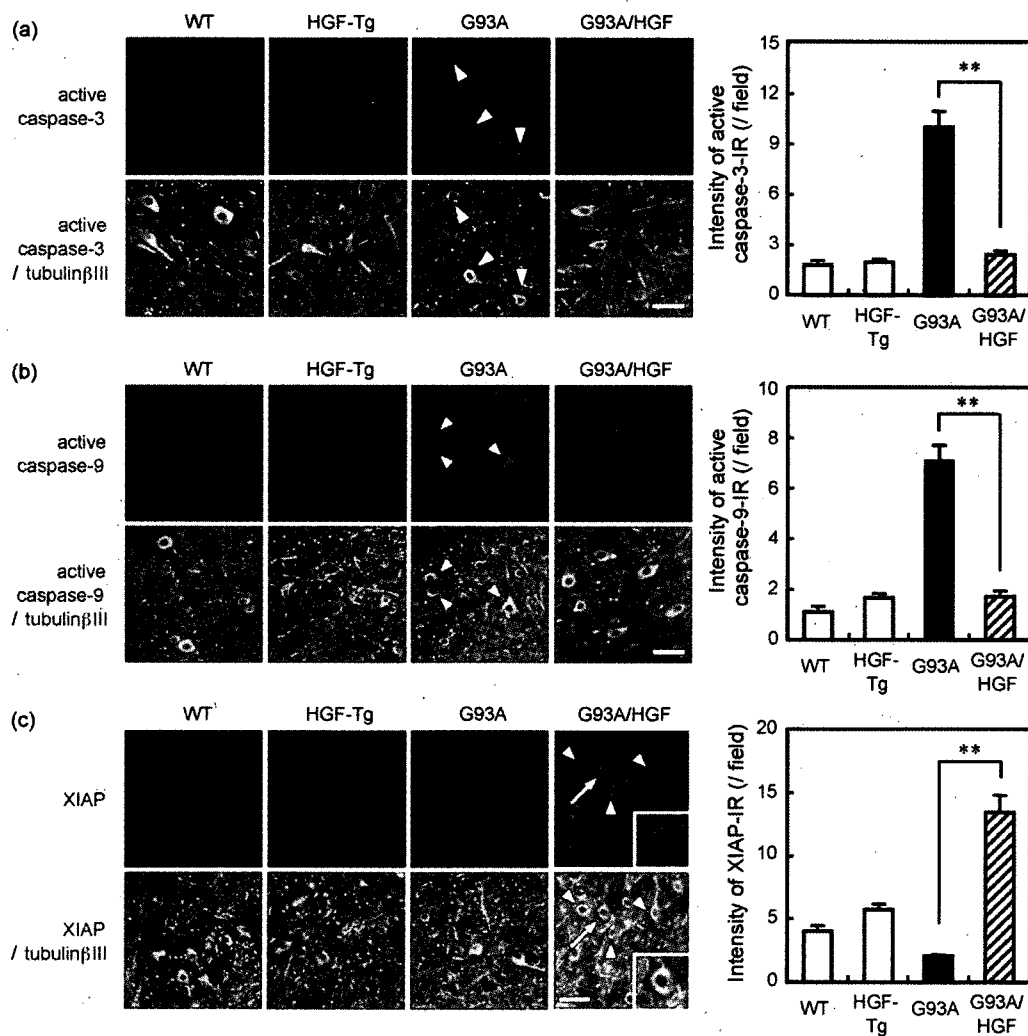

Fig. 5. Attenuation of pro-apoptotic protein activation in the facial motoneurons of G93A/HGF mice. (a) Left panel, double immunofluorescence analysis of active caspase-3 (red) and tubulinßIII (green) in the facial nucleus of WT, HGF-Tg, G93A and G93A/HGF mice at 6 months of age. Active caspase-3-positive neurons, indicated by arrowheads, are evident. Right panel, the intensity of active caspase-3-IR is shown in the facial nucleus of WT, HGF-Tg, G93A and G93A/HGF mice. Data represent the mean ± S.E. (n = 4 for each group). **P < 0.01 vs. G93A mice. (b) Left panel, double immunofluorescence analysis of active caspase-9 (red) and tubulinßIII (green) in the facial nucleus of WT, HGF-Tg, G93A and G93A/HGF mice at 6 months of age. Active caspase-9-positive neurons are indicated by arrowheads. Right panel, the intensity of active caspase-9-IR is shown in the facial nucleus of WT, HGF-Tg, G93A and G93A/HGF mice. Data represent the mean ± S.E. (n = 4 for each group). **P < 0.01 vs. G93A mice. (c) Left panel, double immunofluorescence analysis for XIAP (red) and tubulinßIII (green) in the facial nucleus of WT, HGF-Tg, G93A and G93A/HGF mice at 6 months of age. XIAP-positive neurons are indicated by arrowheads. A high-magnification view of the area indicated by the arrow is also shown for G93A/HGF mice. Scale bars = 50 μm. Right panel, the intensity of XIAP-IR is shown in the facial nucleus of WT, HGF-Tg, G93A and G93A/HGF mice. Data represent the mean ± S.E. (n = 4 for each group). **P < 0.01 vs. G93A mice.

respectively) relative to WT mice. Meanwhile, the mean intensities of active caspase-3-IR and caspase-9-IR in the facial nuclei of G93A/HGF mice were decreased, and were at almost the same level as in WT mice (Fig. 5a and b, right panel). Similar results were obtained for the hypoglossal motoneurons (data not shown). These results suggest that HGF-dependent prevention of facial and hypoglossal motoneuron degeneration in G93A mice was mediated, at least in part, by inhibition of caspase-dependent neuronal cell death.

X chromosome-linked inhibitor of apoptosis protein (XIAP) is a member of a family of protein inhibitors of apoptosis. The protein antagonizes the caspase cascade through direct inhibition of the activation of caspases-3, -7 and -9 (Deveraux et al., 1997). Therefore, the ability of HGF to modify expression of XIAP in facial and hypoglossal nuclei was examined. Immunofluorescence analysis revealed that XIAP-IR was markedly induced in facial motoneurons of G93A/HGF mice at 6 months of age, while the signal was low in WT and HGF-Tg mice, and below the detection limit in G93A mice (Fig. 5c, left panel). The mean intensity of XIAP-IR in the facial nuclei of G93A/HGF mice increased significantly to 6.4-fold over G93A mice. Similar results were obtained for the hypoglossal motoneurons (data not shown). These results suggest that, in addition to attenuation of

caspase-1 activation, HGF induced XIAP expression in the presence of ALS-toxicity.

4. Discussion

4.1. HGF suppresses gliosis in facial and hypoglossal nuclei of a transgenic mouse model of ALS

ALS is characterized by a selective degeneration of motoneurons, regardless of the type of causal mutation or whether the disease is familial or sporadic. Most efforts have been directed toward the prevention of motoneuronal degeneration. However, several studies have suggested that gliosis in the vicinity of degenerating motoneurons may contribute to ALS disease progression, raising the possibility that gliosis might be a good target for curative efforts. In this regard, a single factor with neurotrophic and gliosis-suppressing activities may be beneficial for curing ALS. This study provides the first evidence that introduction of HGF into the nervous system suppresses induction of microglial accumulation in the facial and hypoglossal nuclei of G93A mice at 8 months of age, in addition to its suppressive activity on astrocytosis, using double transgenic mice overexpressing SOD1^{G93A} and HGF. It was recently reported that using the
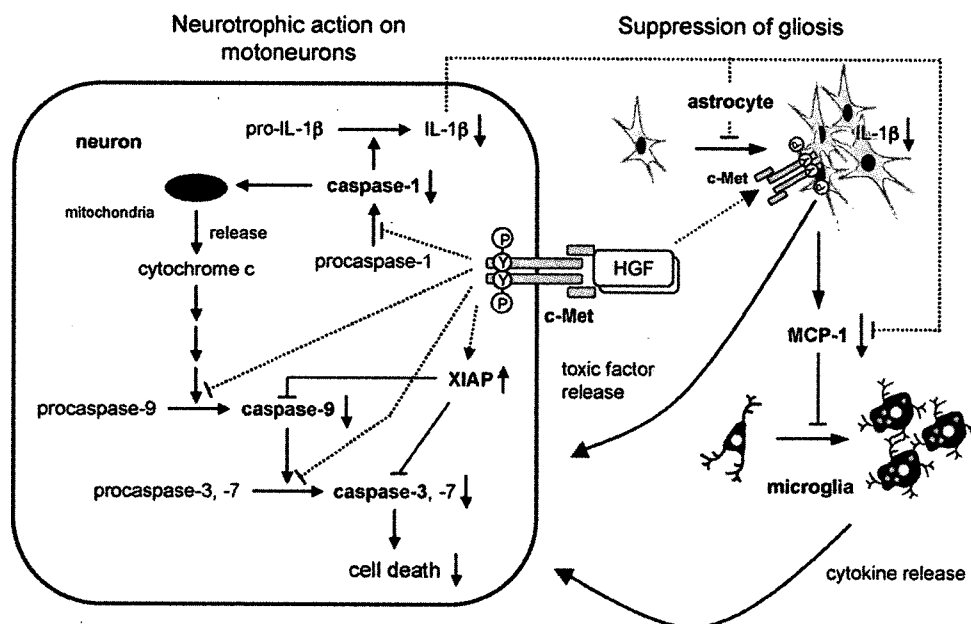

Fig. 6. Proposed working model of the molecular mechanisms of the neuroprotective effect of HGF on G93A mice are shown. In the motoneurons of G93A/HGF mice, HGF binds to c-Met on cell surface and induces autophosphorylation of the intracellular tyrosine residues of c-Met. Subsequently, HGF inhibits caspase-1 activation, induces XIAP and inhibits its downstream caspases, caspase-3, -7 and -9, thereby effectively dampening caspase-dependent cascades. Therefore, the neurotrophic action of HGF on motoneurons is, at least in part, promoted by preventing caspase-mediated cell death signals, which are commonly activated in patients with SALS and FALS, and in G93A mice. In addition to the neuroprotective effect of HGF on motoneurons, HGF also suppresses microglial accumulation, which is contributed in the progression of motoneuronal degeneration by producing cytotoxic cytokines, in G93A mice. By inhibition of caspase-1 activation in motoneurons and, presumably, the subsequent reduction of IL-1ß levels, HGF also suppresses MCP-1 induction in motoneurons and reactive astrocytes, and suppresses microgliosis as well as astrocytosis. HGF-induced attenuation of MCP-1 induction, which is thought to be responsible for the recruitment of monocytic lineage cells including microglia (Meeuwsen et al., 2003), might aid in the lessening of microglial accumulation in the brainstem, thereby presumably leading to a reduction of cytokine release from accumulated microglia (Weydt et al., 2004). The direct function of HGF on astrocytes may also play an important role, since c-Met is induced in reactive spinal cord astrocytes of G93A mice. Furthermore, recent study has reported that astrocytes contribute to motoneuronal degeneration by releasing toxic factors selectively to motoneurons (Nagai et al., 2007; Di Giorgio et al., 2007), suggesting that suppressing effects of HGF on astrocytosis is also advantageous for the treatment of brainstem and spinal motoneurons of ALS patients. In addition, other mechanisms may be involved in the neurotrophic activity and gliosis suppressing activity of HGF.

Cre-lox system to decrease expression of the mutant $SOD1^{G37R}$ transgene by only 25% in microglia of a transgenic mouse model of ALS significantly prolongs disease duration (Boillee et al., 2006). In microglia/motoneuron co-cultures, microglia that express mutant $SOD1^{G93A}$ induce more motoneuron death and decrease neurite numbers and length compared with wild-type microglia (Xiao et al., 2007). Therefore, even a small reduction in the number of disease progressing cells (microglia expressing mutant $SOD1^{G93A}$) (i.e., a small reduction of microglial accumulation) may be beneficial for retarding progression of the disease. It can be postulated that the attenuation of microglial accumulation to 60% in the facial and hypoglossal nuclei of G93A/HGF mice compared with those of G93A mice (Fig. 3a) might be sufficient to affect the disease. This raises the possibility that HGF application would be valuable for ALS therapy with respect to the reduction of microglial accumulation and subsequent disease progression.

The precise mechanism by which HGF attenuates microglial accumulation has not been elucidated. However, the present findings suggest two possibilities. The first possible mechanism is inhibition of caspase-1 activation in motoneurons, which in turn inhibits proteolytic cleavage of pro-IL-1ß to IL-1ß through active caspase-1 (Thornberry et al., 1992). The subsequent suppression of IL-1ß-dependent induction of MCP-1 mRNA is thought to be crucial for recruiting monocytic cells, such as microglia (Meeuwsen et al., 2003) (Fig. 6). In the present study, caspase-1 activation in motoneurons and MCP-1 induction in reactive astrocytes of the facial and hypoglossal nuclei of G93A mice were markedly suppressed in G93A/HGF mice (Fig. 4). Thus, it seems likely that HGF suppresses microglial accumulation by decreasing IL-1ß levels through inhibition of caspase-1 activation in motoneurons and reduction of MCP-1 levels in reactive astrocytes of the facial and hypoglossal nuclei of G93A mice, thereby preventing synergism between microglial accumulation and astrocytosis (Fig. 6). In addition to its effect through motoneurons, it seems likely that HGF directly acts on c-Met expressed in astrocytes to reduce IL-1β and MCP-1 levels, in turn ameliorating astrocytosis and microgliosis. Support for this supposition is evidenced by elevated c-Met levels in spinal cord astrocytes of G93A mice at the end stage of the disease (Sun et al., 2002; data not shown), and by HGF suppression of MCP-1 in the tubular epithelial cells (TEC) of the kidney via an NF-kB-mediated process (Gong et al., 2004). Indeed, upregulation of IL-1β in both spinal motoneurons and reactive astrocytes of G93A mice at 7 months of age is largely attenuated in G93A/HGF mice (Ohya and Funakoshi, unpublished data). Therefore, HGF may suppress gliosis via direct and indirect activities on glial cells. In addition to the above mechanisms, other mechanisms may be involved in the HGF-dependent suppression of microglial accumulation, and such possibilities are under the investigation.

Recent *in vitro* studies provided evidence that astrocytes expressing mutant SOD1 contribute to motoneuronal degeneration mediated by the release of soluble factors that are toxic to degenerate primary motoneurons or motoneurons that are derived from ES cells of mutant SOD1 mice (Nagai et al., 2007;

Di Giorgio et al., 2007). In addition to suppressing microglial accumulation, HGF also suppresses astrocytosis in the facial and hypoglossal nuclei of G93A mice. These results raise the possibility that one of the molecular mechanisms by which HGF prevents motoneuronal degeneration is mediated by suppressing both microglial accumulation and astrocytosis.

4.2. Molecular mechanism of HGF neuroprotective effect on facial and hypoglossal motoneurons against ALS-toxicity

Caspases are activated in the spinal motoneurons of G93A mice, and a dominant negative inhibitor of the IL-1ß-converting enzyme (ICE)/caspase-1, anti-apoptotic protein Bcl-2 and a broad caspase inhibitor, zVAD-fmk, significantly slow the onset of ALS in a transgenic mouse model (Friedlander et al., 1997; Kostic et al., 1997; Pasinelli et al., 2000; Li et al., 2000; Guegan et al., 2001; Inoue et al., 2003). The results of the present study provide evidence that caspase-1, -3 and -9 are activated in facial and hypoglossal motoneurons of G93A mice, while their activation is suppressed in G93A/HGF mice (Figs. 4b, 5 and 6). These results suggest that the effects of HGF on caspase-dependent apoptosis in motoneurons may retard the early disease process.

Independent of its caspase-1 inhibition function, the upregulation of XIAP in brainstem motoneurons by HGF may also be beneficial in retarding the disease. XIAP functions as a ubiquitin ligase toward mature caspase-9 and second mitochondria-derived caspase activator (Smac), which is also known as direct IAP binding protein with low PI (DIABLO) and promotes caspase activation in the caspase-9 pathway by binding IAPs and preventing them from inhibiting caspases (Shi, 2004), to inhibit apoptosis (Morizane et al., 2005). Inoue et al. (2003) reported that gene transfer of XIAP attenuates disease progression without delaying onset through inhibition of caspase-9 activation in G93A mice, suggesting that caspase-9 contributes to the duration of the disease. Collectively, the actions of HGF cause not only caspase-1 inhibition, but also upregulation of XIAP and inhibition of its downstream caspases in brainstem motoneurons. These actions of HGF may be, at least in part, involved in the mechanisms associated with retarding disease onset and duration, and prolonging the lifespan in the familial ALS (FALS) mouse model. We previously reported that HGF delays onset and prolongs lifespan, but does not extend duration in G93A mice due to insufficient delivery of HGF in the late stages (Sun et al., 2002). Thus, improved delivery of HGF may further enhance its effect at later stages of ALS.

Immunocytochemical, Western blotting and DNA micro-array analyses have shown that caspase expression is upregulated in patients with sporadic ALS (SALS) and/or FALS compared with non-ALS controls (Ilzecka et al., 2001; Inoue et al., 2003; Calingasan et al., 2005; Jiang et al., 2005). These results suggest that activation of these caspases may be a common pathway of disease progression for both FALS and SALS. Furthermore, in both SALS and FALS patients, HGF and c-Met are regulated in a manner similar to that seen in

FALS mice (Kato et al., 2003). Therefore, HGF delays onset and may prolong disease duration through inhibition of a common caspase-dependent pathway in ALS. Post-diagnostic HGF therapy could be considered not only for mutant SOD1-related FALS, but also for SALS.

4.3. HGF may be an effective agent for ALS therapy

Since motoneuronal death is the major and common characteristic of both FALS and SALS (Cleveland and Rothstein, 2001), neurotrophic factors have been proposed as highly potent therapeutic agents for motoneuronal degeneration (Sendtner et al., 1992; Funakoshi et al., 1995, 1998; Wang et al., 2002; Sun et al., 2002; Kaspar et al., 2003; Azzouz et al., 2004). Some neurotrophic factors, including HGF, glial cell-line derived neurotrophic factor (GDNF), insulin-like growth factor-1 (IGF-1), and vascular endothelial growth factor (VEGF), confer neuroprotective properties to spinal motoneurons in a transgenic mouse model of ALS (present study; Sun et al., 2002; Wang et al., 2002; Kaspar et al., 2003; Azzouz et al., 2004), raising the possibility of their use as therapeutics. However, some neurotrophic factors may not prevent the death of subpopulations of spinal cord and brainstem motoneurons under degenerative conditions, including ALS-toxicity (Sakamoto et al., 2003; Guillot et al., 2004). The effects of these factors on brainstem motoneurons in the transgenic mouse model of ALS are not well understood. The finding that HGF is capable of attenuating motoneuronal death in both brainstem (present study) and spinal motoneurons (Sun et al., 2002), might be useful in future therapeutic applications of HGF in ALS patients. The potential of HGF to decrease gliosis, including microglial accumulation, in addition to its direct neurotrophic activity on motoneurons might be of further benefit.

In summary, this study provides the first evidence that HGF exerts a neuroprotective effect on facial and hypoglossal motoneurons against ALS-toxicity by preventing motoneuronal death via suppression of pro-apoptotic protein activation and by reducing gliosis via inhibition of MCP-1 induction. Although development of a delivery method for the HGF protein and gene may be required before clinical application, these findings suggest that HGF may be an effective therapeutic agent for the treatment of brainstem and spinal motoneurons in ALS patients.

Acknowledgements

References

Azzouz, M., Ralph, G.S., Storkebaum, E., Walmsley, L.E., Mitrophanous, K.A., Kingsman, S.M., Carmeliet, P., Mazarakis, N.D., 2004. VEGF delivery with retrogradely transported lentivector prolongs survival in a mouse ALS model. Nature 429, 413–417.

Baron, P., Bussini, S., Cardin, V., Corbo, M., Conti, G., Galimberti, D., Scarpini, E., Bresolin, N., Wharton, S.B., Shaw, P.J., Silani, V., 2005. Production of monocyte chemoattractant protein-1 in amyotrophic lateral sclerosis. Muscle Nerve 32, 541–544.

Berman, J.W., Guida, M.P., Warren, J., Amat, J., Brosnan, C.F., 1996. Localization of monocyte chemoattractant peptide-1 expression in the central nervous system in experimental autoimmune encephalomyelitis and trauma in the rat. J. Immunol. 156, 3017–3023.

Boillee, S., Yamanaka, K., Lobsiger, C.S., Copeland, N.G., Jenkins, N.A., Kassiotis, G., Kollias, G., Cleveland, D.W., 2006. Onset and progression in inherited ALS determined by motor neurons and microglia. Science 312, 1389–1392.

Calingasan, N.Y., Chen, J., Kiaei, M., Beal, M.F., 2005. β-Amyloid 42 accumulation in the lumbar spinal cord motor neurons of amyotrophic lateral sclerosis patients. Neurobiol. Dis. 19, 340–347.

Cleveland, D.W., Rothstein, J.D., 2001. From Charcot to Lou Gehrig: deciphering selective motor neuron death in ALS. Nat. Rev. Neurosci. 2, 806–819.

Deveraux, Q.L., Takahashi, R., Salvesen, G.S., Reed, J.C., 1997. X-linked IAP is a direct inhibitor of cell-death proteases. Nature 388, 300–304.

Di Giorgio, F.P., Carrasco, M.A., Siao, M.C., Maniatis, T., Eggan, K., 2007. Non-cell autonomous effect of glia on motor neurons in an embryonic stem cell-based ALS model. Nat. Neurosci. 10, 608–614.

Ebens, A., Brose, K., Leonardo, E.D., Hanson Jr., M.G., Bladt, F., Birchmeier, C., Barres, B.A., Tessier-Lavigne, M., 1996. Hepatocyte growth factor/scatter factor is an axonal chemoattractant and a neurotrophic factor for spinal motor neurons. Neuron 17, 1157–1172.

Friedlander, R.M., Brown, R.H., Gagliardini, V., Wang, J., Yuan, J., 1997. Inhibition of ICE slows ALS in mice. Nature 388, 31.

Funakoshi, H., Belluardo, N., Arenas, E., Yamamoto, Y., Casabona, A., Persson, H., Ibanez, C.F., 1995. Muscle-derived neurotrophin-4 as an activity-dependent trophic signal for adult motor neurons. Science 268, 1495–1499.

Funakoshi, H., Risling, M., Carlstedt, T., Lendahl, U., Timmusk, T., Metsis, M., Yamamoto, Y., Ibanez, C.F., 1998. Targeted expression of a multifunctional chimeric neurotrophin in the lesioned sciatic nerve accelerates regeneration of sensory and motor axons. Proc. Natl. Acad. Sci. U.S.A. 95, 5269–5274.

Funakoshi, H., Nakamura, T., 2003. Hepatocyte growth factor: from diagnosis to clinical applications. Clin. Chim. Acta 327, 1–23.

Giulian, D., Woodward, J., Young, D.G., Krebs, J.F., Lachman, L.B., 1988. Interleukin-1 injected into mammalian brain stimulates astrocytosis and neovascularization. J. Neurosci. 8, 2485–2490.

Gong, R., Rifai, A., Tolbert, E.M., Biswas, P., Centracchio, J.N., Dworkin, L.D., 2004. Hepatocyte growth factor ameliorates renal interstitial inflammation in rat remnant kidney by modulating tubular expression of macrophage chemoattractant protein-1 and RANTES. J. Am. Soc. Nephrol. 15, 2868–2881.

Guegan, C., Vila, M., Rosoklija, G., Hays, A.P., Przedborski, S., 2001. Recruitment of the mitochondrial-dependent apoptotic pathway in amyotrophic lateral sclerosis. J. Neurosci. 21, 6569–6576.

Guillot, S., Azzouz, M., Deglon, N., Zurn, A., Aebischer, P., 2004. Local GDNF expression mediated by lentiviral vector protects facial nerve motor neurons but not spinal motor neurons in SOD1(G93A) transgenic mice. Neurobiol. Dis. 16, 139–149.

Gurney, M.E., Pu, H., Chiu, A.Y., Dal Canto, M.C., Polchow, C.Y., Alexander, D.D., Caliendo, J., Hentati, A., Kwon, Y.W., Deng, H.X., Chen, W., Zhai, P., Sufit, R.L., Siddique, T., 1994. Motor neuron degeneration in mice that express a human Cu, Zn superoxide dismutase mutation. Science 264, 1772–1775.

Henkel, J.S., Engelhardt, J.I., Siklos, L., Simpson, E.P., Kim, S.H., Pan, T., Goodman, J.C., Siddique, T., Beers, D.R., Appel, S.H., 2004. Presence of dendritic cells, MCP-1, and activated microglia/macrophages in amyotrophic lateral sclerosis spinal cord tissue. Ann. Neurol. 55, 221–235.

Henkel, J.S., Beers, D.R., Siklos, L., Appel, S.H., 2006. The chemokine MCP-1 and the dendritic and myeloid cells it attracts are increased in the mSOD1 mouse model of ALS. Mol. Cell. Neurosci. 31, 427–437.

Herx, L.M., Yong, V.W., 2001. Interleukin-1β is required for the early evolution of reactive astrocytosis following CNS lesion. J. Neuropathol. Exp. Neurol. 60, 961–971.

Honda, S., Kagoshima, M., Wanaka, A., Tohyama, M., Matsumoto, K., Nakamura, T., 1995. Localization and functional coupling of HGF and c-Met/HGF receptor in rat brain: implication as neurotrophic factor. Brain Res. Mol. Brain Res. 32, 197–210.

Ilzecka, J., Stelmasiak, Z., Dobosz, B., 2001. Interleukin-1ß converting enzyme/ Caspase-1 (ICE/Caspase-1) and soluble APO-1/Fas/CD 95 receptor in amyotrophic lateral sclerosis patients. Acta Neurol. Scand. 103, 255–258.

Imai, Y., Ibata, I., Ito, D., Ohsawa, K., Kohsaka, S., 1996. A novel gene iba1 in the major histocompatibility complex class III region encoding an EF hand protein expressed in a monocytic lineage. Biochem. Biophys. Res. Commun. 224, 855–862.

Inoue, H., Tsukita, K., Iwasato, T., Suzuki, Y., Tomioka, M., Tateno, M., Nagao, M., Kawata, A., Saido, T.C., Miura, M., Misawa, H., Itohara, S., Takahashi, R., 2003. The crucial role of caspase-9 in the disease progression of a transgenic ALS mouse model. EMBO J. 22, 6665–6674.

Jiang, Y.M., Yamamoto, M., Kobayashi, Y., Yoshihara, T., Liang, Y., Terao, S., Takeuchi, H., Ishigaki, S., Katsuno, M., Adachi, H., Niwa, J., Tanaka, F., Doyu, M., Yoshida, M., Hashizume, Y., Sobue, G., 2005. Gene expression profile of spinal motor neurons in sporadic amyotrophic lateral sclerosis. Ann. Neurol. 57, 236–251.

John, G.R., Chen, L., Rivieccio, M.A., Melendez-Vasquez, C.V., Hartley, A., Brosnan, C.F., 2004. Interleukin-1ß induces a reactive astroglial phenotype via deactivation of the Rho GTPase-Rock axis. J. Neurosci. 24, 2837–2845.

Kaspar, B.K., Llado, J., Sherkat, N., Rothstein, J.D., Gage, F.H., 2003. Retrograde viral delivery of IGF-1 prolongs survival in a mouse ALS model. Science 301, 839–842.

Kato, S., Funakoshi, H., Nakamura, T., Kato, M., Nakano, I., Hirano, A., Ohama, E., 2003. Expression of hepatocyte growth factor and c-Met in the anterior horn cells of the spinal cord in the patients with amyotrophic lateral sclerosis (ALS): immunohistochemical studies on sporadic ALS and familial ALS with superoxide dismutase 1 gene mutation. Acta Neuropathol. 106, 112–120.

Keep, M., Elmer, E., Fong, K.S., Csiszar, K., 2001. Intrathecal cyclosporin prolongs survival of late-stage ALS mice. Brain Res. 894, 327–331.

Kostic, V., Jackson-Lewis, V., de Bilbao, F., Dubois-Dauphin, M., Przedborski, S., 1997. Bcl-2: prolonging life in a transgenic mouse model of familial amyotrophic lateral sclerosis. Science 277, 559–562.

Kriz, J., Nguyen, M.D., Julien, J.P., 2002. Minocycline slows disease progression in a mouse model of amyotrophic lateral sclerosis. Neurobiol. Dis. 10, 268–278.

Li, M., Ona, V.O., Guegan, C., Chen, M., Jackson-Lewis, V., Andrews, L.J., Olszewski, A.J., Stieg, P.E., Lee, J.P., Przedborski, S., Friedlander, R.M., 2000. Functional role of caspase-1 and caspase-3 in an ALS transgenic mouse model. Science 288, 335–339.

Meeuwsen, S., Persoon-Deen, C., Bsibsi, M., Ravid, R., van Noort, J.M., 2003. Cytokine, chemokine and growth factor gene profiling of cultured human astrocytes after exposure to proinflammatory stimuli. Glia 43, 243–253.

Morizane, Y., Honda, R., Fukami, K., Yasuda, H., 2005. X-linked inhibitor of apoptosis functions as ubiquitin ligase toward mature caspase-9 and cytosolic Smac/DIABLO. J. Biochem. (Tokyo) 137, 125–132.

Nagai, M., Re, D.B., Nagata, T., Chalazonitis, A., Jessell, T.M., Wichterle, H., Przedorski, S., 2007. Astrocytes expressing ALS-linked mutated SOD1 release factors selectively toxic to motor neurons. Nat. Neurosci. 10, 615–622.

Nakamura, T., Nawa, K., Ichihara, A., 1984. Partial purification and characterization of hepatocyte growth factor from serum of hepatectomized rats. Biochem. Biophys. Res. Commun. 122, 1450–1459.

Nakamura, T., Nishizawa, T., Hagiya, M., Seki, T., Shimonishi, M., Sugimura, A., Tashiro, K., Shimizu, S., 1989. Molecular cloning and expression of human hepatocyte growth factor. Nature 342, 440–443.

Novak, K.D., Prevette, D., Wang, S., Gould, T.W., Oppenheim, R.W., 2000. Hepatocyte growth factor/scatter factor is a neurotrophic survival factor for lumbar but not for other somatic motor neurons in the chick embryo. J. Neurosci. 20, 326–337.

Pasinelli, P., Houseweart, M.K., Brown Jr., R.H., Cleveland, D.W., 2000. Caspase-1 and -3 are sequentially activated in motor neuron death in Cu, Zn superoxide dismutase-mediated familial amyotrophic lateral sclerosis. Proc. Natl. Acad. Sci. U.S.A. 97, 13901–13906.

Pasinelli, P., Brown Jr., R.H., 2006. Molecular biology of amyotrophic lateral sclerosis: insights from genetics. Nat. Rev. Neurosci. 7, 710–723.

Sakamoto, T., Kawazoe, Y., Shen, J.S., Takeda, Y., Arakawa, Y., Ogawa, J., Oyanagi, K., Ohashi, T., Watanabe, K., Inoue, K., Eto, Y., Watabe, K., 2003. Adenoviral gene transfer of GDNF, BDNF and TGF beta 2, but not CNTF, cardiotrophin-1 or IGF1, protects injured adult motor neurons after facial nerve avulsion. J. Neurosci. Res. 72, 54–64.

Sendtner, M., Holtmann, B., Kolbeck, R., Thoenen, H., Barde, Y.A., 1992. Brain-derived neurotrophic factor prevents the death of motor neurons in newborn rats after nerve section. Nature 360, 757–759.

Shi, Y., 2004. Caspase activation, inhibition, and reactivation: a mechanistic view. Protein Sci. 13, 1979–1987.

Sun, W., Funakoshi, H., Nakamura, T., 2002. Overexpression of HGF retards disease progression and prolongs life span in a transgenic mouse model of ALS. J. Neurosci. 22, 6537–6548.

Thornberry, N.A., Bull, H.G., Calaycay, J.R., Chapman, K.T., Howard, A.D., Kostura, M.J., Miller, D.K., Molineaux, S.M., Weidner, J.R., Aunins, J., Elliston, K.O., Ayala, J.M., Casano, F.J., Chin, J., Ding, G.J.F., Egger, L.A., Gaffney, E.P., Limjuco, G., Palyha, O.C., Raju, S.M., Rolando, A.M., Salley, J.P., Yamin, T.-T., Lee, T.D., Shively, J.E., MacCross, M., Mumford, R.A., Schmidt, J.A., Tocci, M.J., 1992. A novel heterodimeric cysteine protease is required for interleukin-1ß processing in monocytes. Nature 356, 768–774.

Van Den Bosch, L., Tilkin, P., Lemmens, G., Robberecht, W., 2002. Minocycline delays disease onset and mortality in a transgenic model of ALS. Neuroreport 13, 1067–1070.

Wang, L.J., Lu, Y.Y., Muramatsu, S., Ikeguchi, K., Fujimoto, K., Okada, T., Mizukami, H., Matsushita, T., Hanazono, Y., Kume, A., Nagatsu, T., Ozawa, K., Nakano, I., 2002. Neuroprotective effects of glial cell line-derived neurotrophic factor mediated by an adeno-associated virus vector in a transgenic animal model of amyotrophic lateral sclerosis. J. Neurosci. 22, 6920–6928.

Weydt, P., Yuen, E.C., Ransom, B.R., Moller, T., 2004. Increased cytotoxic potential of microglia from ALS-transgenic mice. GLIA 48, 179–182.

Xiao, Q., Zhao, W., Beers, D.R., Yen, A.A., Xie, W., Henkel, J.S., Appel, S.H., 2007. Mutant SOD1G93A microglia are more neurotoxic relative to wildtype microglia. J. Neurochem. 102, 2008–2019.

Yamamoto, Y., Livet, J., Pollock, R.A., Garces, A., Arce, V., deLapeyriere, O., Henderson, C.E., 1997. Hepatocyte growth factor (HGF/SF) is a muscle-derived survival factor for a subpopulation of embryonic motor neurons. Development 124, 2903–2913.

Yrjanheikki, J., Tikka, T., Keinanen, R., Goldsteins, G., Chan, P.H., Koistinaho, J., 1999. A tetracycline derivative, minocycline, reduces inflammation and protects against focal cerebral ischemia with a wide therapeutic window. Proc. Natl. Acad. Sci. U.S.A. 96, 13496–13500.

Zhu, S., Stavrovskaya, I.G., Drozda, M., Kim, B.Y., Ona, V., Li, M., Sarang, S., Liu, A.S., Hartley, D.M., Wu, D.C., Gullans, S., Ferrante, R.J., Przedborski, S., Kristal, B.S., Friedlander, R.M., 2002. Minocycline inhibits cytochrome c release and delays progression of amyotrophic lateral sclerosis in mice. Nature 417, 74–78.

BRAIN
RESEARCH

ELSEVIER

Research Report

Hepatocyte growth factor (HGF) promotes oligodendrocyte progenitor cell proliferation and inhibits its differentiation during postnatal development in the rat

Wakana Ohya[a], Hiroshi Funakoshi[a], Tsutomu Kurosawa[b], Toshikazu Nakamura[a],*

[a]Division of Molecular Regenerative Medicine, Department of Biochemistry and Molecular Biology, Osaka University Graduate School of Medicine, B-7, Osaka 565-0871, Japan
[b]Institute of Experimental Animal Sciences, Osaka University Graduate School of Medicine, Osaka 565-0871, Japan

ARTICLE INFO

ABSTRACT

Hepatocyte growth factor (HGF) was initially cloned as a mitogen for hepatocytes and has been identified as a neurotrophic factor for a variety of neurons. However, few attempts have assessed the role of HGF in cells of oligodendrocyte lineage. The purpose of this study was to elucidate the role of HGF in such cells during development. Double immunostaining for either c-Met/HGF receptor or phospho-c-Met with either NG2 or RIP in rat striatum at postnatal day 3 (P3), P7, and P14 revealed that c-Met was phosphorylated on tyrosine residues and thereby activated in NG2$^+$ oligodendrocyte progenitor cells (OPCs) at P3-P14 and in RIP$^+$ oligodendrocytes at P14. Intrastriatal injections of recombinant human HGF at both P7 and P10 revealed that the relative ratio of BrdU$^+$/NG2$^+$ cells per total number of NG2$^+$ cells increased, while BrdU$^+$/MBP$^+$ oligodendrocyte numbers decreased. Western blot analysis showed a down-regulation of myelin basic protein (MBP) after HGF injection. Electron microscopy revealed that the numbers of myelinated nerve fibers decreased after HGF treatment. Furthermore, administration of anti-HGF IgG into the striatum increased the number of BrdU$^+$/MBP$^+$ oligodendrocytes. These findings demonstrated that HGF increases proliferation of OPCs and attenuates their differentiation into myelinating oligodendrocytes, presumably by favoring neurite outgrowth that may be inhibited by the myelin inhibitory molecules on oligodendrocytes. Down-regulation of HGF mRNA in the striatum from P7 to P14, as revealed by quantitative real-time RT-PCR, may be favorable for OPC differentiation into myelinating oligodendrocytes. Our findings suggest that c-Met signaling, together with HGF regulation, plays an important role in developmental oligodendrogenesis.

1. Introduction

Proliferation, differentiation, and maturation of oligodendrocyte progenitor cells (OPCs) and oligodendrocytes, together with their mutual communication with neurons, are essential for the functional development of the nervous system. These events are tightly and precisely regulated by the communication of developing oligodendrocyte lineage cells with surround-

ing cells, such as astrocytes and neuronal axons, especially during postnatal development. It has been shown that two different notch signaling pathways play a critical role in the switching of OPCs from a proliferation state to a differentiation state at postnatal day 6 (P6) in rodents (Hu et al., 2003; Hu et al., 2006). Prior to P6, the astrocyte-expressed Jagged1 protein transactivates OPCs to induce intracellular notch signaling via Hairy Enhancer of Split-1 (HES-1), which contributes to the maintenance of OPCs in an undifferentiated state (Wang et al., 1998). However, Jagged1 expression sharply decreases at P6, a time point concurrent with the onset of myelination, and its inhibitory activity toward OPC differentiation becomes weak. On the other hand, after P6, levels of the axon-derived notch ligand "F3/contactin" increase, which in turn transactivate OPCs, inducing a second intracellular notch signaling molecule "Deltex1", which contributes to OPC differentiation into mature oligodendrocytes. Therefore, the switch from a proliferation state to a differentiation state is dependent upon the two different notch pathways, "Jagged1/notch/HES-1" and "contactin/notch/Deltex1" (Hu et al., 2003). In addition, other factors, such as platelet-derived growth factor (PDGF) and fibroblast growth factor-2 (FGF2), have been found to be partially involved in these processes during either development or adulthood (Bogler et al., 1990; Butt and Dinsdale, 2005b; McKinnon et al., 1990). While FGF2 is known to be involved in the induction of demyelination in adult CNS (Butt and Dinsdale, 2005a), the molecular mechanisms by which OPCs proliferate, differentiate, and mature during the course of development are still not fully understood.

Hepatocyte growth factor (HGF) was initially identified and cloned as a mitogen for primary hepatocytes (Nakamura et al., 1984, 1989) and was later found to be a novel neurotrophic factor for various types of neurons in both the CNS and PNS (Funakoshi and Nakamura, 2003; Maina et al., 1998), such as hippocampus (Honda et al., 1995), midbrain dopaminergic neurons (Hamanoue et al., 1996), cerebral cortical neurons (Sun et al., 2002a), sensory neurons (Funakoshi and Nakamura, 2001; Maina et al., 1997), motor neurons (Ebens et al., 1996; Yamamoto et al., 1997), cerebellar granular cells (Zhang et al., 2000), and cortical interneurons (Powell et al., 2001) in vitro. HGF was also found to be a neurotrophic factor in vivo in rodent models of brain ischemia (Ishihara et al., 2005; Miyazawa et al., 1998) and motor nerve injuries (Hayashi et al., 2006; Okura et al., 1999). Anxiolytic effects of HGF are also evident (Isogawa et al., 2005). In addition, we found that HGF gene transfer in the neurons of a transgenic mouse model of amyotrophic lateral sclerosis (ALS) overexpressing SOD1^{G93A} attenuates the degeneration of both spinal and brainstem motor neurons, retards the progression of functional motor impairment, and improves the life span of animals with ALS (Sun et al., 2002b) (Kadoyama, Funakoshi et al., unpublished data). Taken together, both the presence and regulation of the HGF-c-Met/HGF receptor system in familial as well as sporadic patients with ALS suggest a physiological role for HGF in retarding the progression of the disease in such patients (Kato et al., 2003). In contrast to its activities on neurons, little information is available on the role of HGF in oligodendrocyte lineage cells, except for in vitro evidence that c-Met is present in both cultured OPCs and oligodendrocytes, and that HGF is capable of accelerating the proliferation of OPCs in culture (Yan and Rivkees, 2002).

As null mutations of both HGF and c-met show embryonic lethality (Bladt et al., 1995; Schmidt et al., 1995; Uehara et al., 1995), making the analysis of the role of HGF in postnatal development difficult, we took advantage of two approaches in the present study to assess the role of HGF in oligodendrogenesis during postnatal development in vivo. First, we used antibodies specific for c-Met as well as antibodies specific for phospho-c-Met, which recognize the intracellular, phosphorylated c-Met tyrosine residues (phospho-Tyr$^{1230/1234/1235}$) for detection of its activation in vivo. Second, we treated animals with recombinant human HGF (rhHGF) or anti-HGF IgG by stereotaxic injection into the striatum and examined the in vivo role of HGF in oligodendrogenesis by immunohistochemistry, Western blotting, and electron microscopy. The results demonstrated that HGF plays an important role in the promotion of both OPC proliferation and attenuation of its differentiation into myelinating oligodendrocytes.

2.   Results

2.1.   c-Met/HGF receptor is present in OPCs and oligodendrocytes during early postnatal development in vivo

In rat striatum, MBP^{+} oligodendrocytes became prominent as dense fiber bundles at P14 compared with P7 (Fig. 1a). NG2^{+} OPCs were evident from P3 to P14 (Fig. 1b), demonstrating the importance of this early postnatal period in both OPC and oligodendrocyte development in the striatum. Therefore, to examine the biological role of HGF in oligodendrocyte development, we first assessed whether c-Met was expressed in oligodendrocyte lineage cells from P3 to P14 by immunostaining using a specific antibody against c-Met. Double fluorescence immunostaining of c-Met and NG2, a marker for OPC, revealed that c-Met^{+}/NG2^{+} immunoreactivity (IR) (green/red) was evident in addition to the large numbers of c-Met single-positive cells at P3 (Fig. 1b, upper panel). At both P7 and P14, NG2 IR overlapped c-Met IR, demonstrating the presence of c-Met IR in OPCs during all postnatal periods examined. It has been reported that NG2 staining overlaps with that of another OPC marker, PDGFRα, in the striatum at P3, and thus NG2 and PDGFRα can serve as reliable markers for the identification of O2A progenitor cells; however, there is a small population of NG2^{+} cells that do not overlap with PDGFRα^{+} cells at late stages of postnatal development (Nishiyama et al., 1996). To further confirm the expression of c-Met in OPCs from the early postnatal striatum, the population of NG2^{+} cells was compared with PDGFRα^{+} cells from P3 to P14. Double immunostaining revealed that NG2^{+} cells overlapped PDGFRα^{+} cells from P3 to P11; NG2^{+} endothelial cells were easily distinguishable from OPCs (Fig. 1c). On the other hand, it should be noted that there is a small population of NG2^{+} cells that does not overlap with PDGFRα^{+} cells in the striatum at P14 (data not shown). The presence of c-Met^{+}/PDGFRα^{+} cells at P14 demonstrated that c-Met is present in OPCs during all developmental stages examined. Double immunostaining for c-Met and RIP, a marker for oligodendrocytes, revealed that c-Met IR was detected in RIP^{+} oligodendrocytes (red) at P14 (Fig. 1b, lower panel). These findings suggest that both OPCs and oligodendrocytes are potential target cells for HGF in the striatum during early postnatal development.

2.2. Numbers of OPCs and oligodendrocytes were reciprocally regulated from P7 to P14

To assess the regulation of oligodendrogenesis from P3 to P14, we examined the number of both PDGFRα[+] (Fig. 2a) and RIP[+] (Fig. 2b) cells since at P14 there is a population of NG2^{+} cells that do not overlap with PDGFRα. The number of PDGFRα[+] OPCs increased from P3 to P7 and decreased from P7 to P14 (Fig. 2a). In contrast, the number of RIP[+] oligodendrocytes

increased from P7 to P14 (Fig. 2b). Double immunostaining of the oligodendrocytic markers and c-Met (Figs. 2c, d) revealed that c-Met was expressed in both PDGFRα[+] OPCs and RIP[+] oligodendrocytes at all developmental stages (from P3 to P14). Therefore, the numbers of OPCs and oligodendrocytes were reciprocally regulated from P7 to P14. Additionally, c-Met is expressed in most populations of OPCs and oligodendrocytes, suggesting that the HGF-c-Met system plays an important role in oligodendrogenesis during early postnatal development.
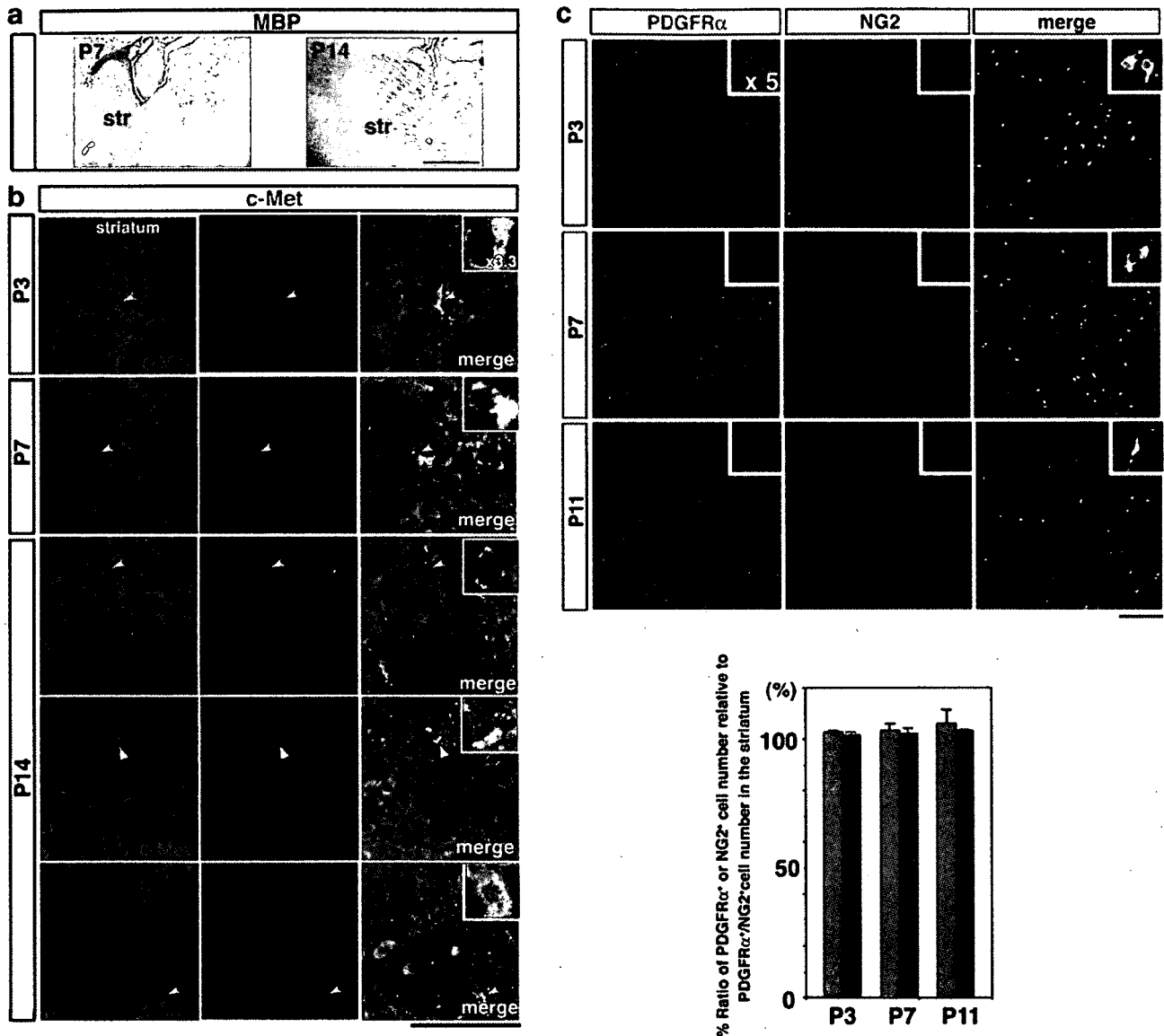
Fig. 1 - c-Met IR is present in NG2^{+} OPCs from P3 to P14 and in RIP[+] oligodendrocytes at P14. (a) Immunostaining for anti-MBP antibody in the sagittal sections of P7 and P14 rat brains. Slides were counterstained with hematoxylin. Only weak MBP IR is detected in the striatum at P7, while strong MBP IR with a cingulated pattern is detected in the striatum at P14. Str, striatum. Scale bar=1 mm. (b) Double fluorescence immunostaining for c-Met (green) and NG2 (red), for c-Met (green) and PDGFRα (red), or for c-Met (green) and RIP (red) (bottom panel) and counterstained with TOPRO-3 iodide (blue) for nuclear staining in P3 (upper panel), P7 (middle panel), and P14 (lower panel) rat striatum. Arrowheads indicate double-immunostained cells with NG2/c-Met, PDGFRα/c-Met, or RIP/c-Met. The insets designate higher (×3.3) magnification views, indicated by arrowheads. Scale bar=100 μm. (c) Double fluorescence immunostaining for PDGFRα (green) and NG2 (red) in the striatum during development (upper panel). Lower panel shows the quantification of the ratio of PDGFRα single-positive cells (green) or NG2 single-positive (red) cells per double-positive cells at P3, P7, and P11. The insets designate higher (×5) magnification views. Scale bar=100 μm.

2.3. Down-regulation of HGF mRNA and protein from P7 to P14 is correlated with a reduction in both the rate of c-Met phosphorylation and of OPC numbers in the striatum

To assess whether the regulation of HGF expression is regulated in accordance with oligodendrogenesis, we determined the levels of HGF mRNA by quantitative real-time RT-PCR in the striatum at both P7 and P14. As shown in Fig. 3a, the relative levels of HGF mRNA, standardized to GAPDH mRNA, decreased from P7 to P14. Immunostaining of HGF revealed that HGF IR was detected at low levels in small neurons of the striatum, while HGF IR was detected at relatively high levels in large neurons (Fig. 3b, upper panel, inset) and blood vessels. In contrast, HGF IR was below the detection limit in PDGFRα⁺ OPCs (Fig. 3b, lower panel). In addition, HGF IR was detected in the striatal matrix with a concentration gradient from the outer surface (higher HGF levels) to the inner side (lower levels) of the striatum. The overall levels of HGF IR slightly decreased from P7 to P14. We next assessed whether the regulation of HGF can contribute to

the activation of c-Met by taking advantage of an anti-phospho-c-Met antibody that specifically recognizes the intracellular phosphorylated tyrosine residues (1230, 1234, and 1235) of c-Met, which reflect HGF intracellular signaling. Immunoprecipitation by c-Met and subsequent Western blotting of both phospho-c-Met and c-Met revealed that the ratio of phospho-c-Met per c-Met in the striatum decreased from P7 to P14 (Fig. 3c). Taken together with the finding that OPC numbers decreased from P7 to P14 (Fig. 2a), our findings suggest that the down-regulation of HGF in the striatum correlates with the reduction of both the endogenous activation rate of c-Met and OPC cell numbers from P7 to P14.

2.4. c-Met is tyrosine phosphorylated and thereby activated in OPCs and oligodendrocytes during early postnatal development in vivo

We next examined which cellular population of oligodendrocyte lineage cells was activated by HGF during postnatal development. NG2 IR (red) overlapped with phospho-c-Met IR
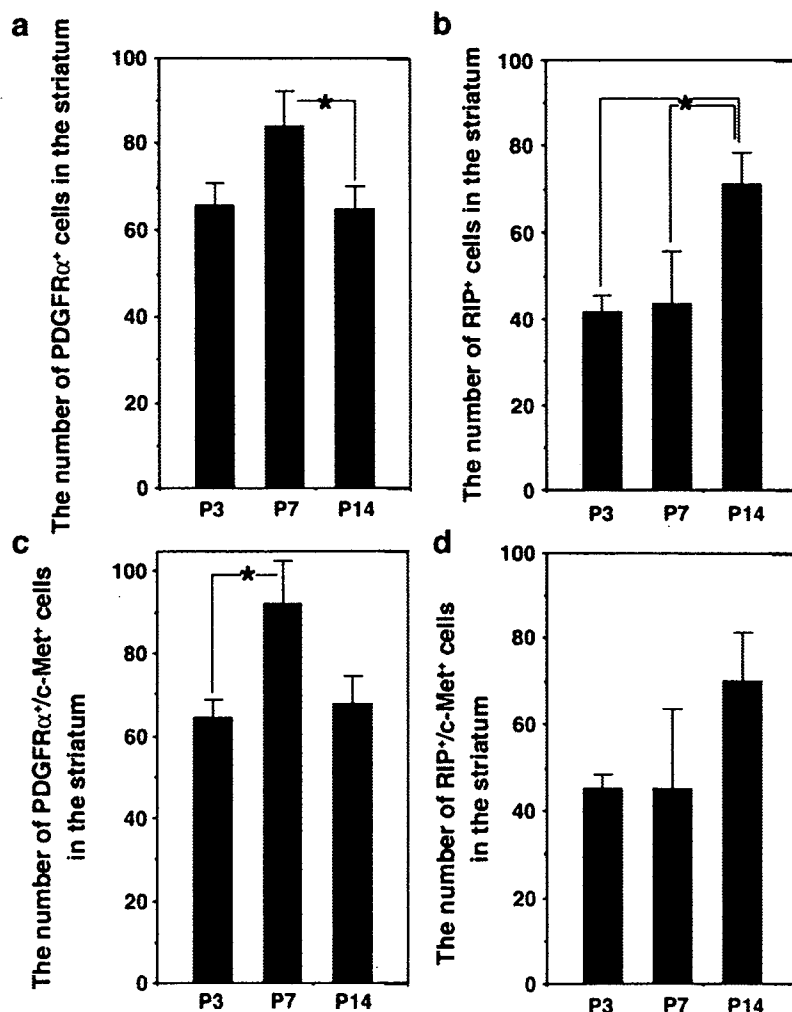

Fig. 2 – The numbers of PDGFRα⁺ OPCs are reciprocally regulated with those of RIP⁺ oligodendrocytes during postnatal development. The numbers of PDGFRα⁺ ($n=6$) (a), RIP⁺ ($n=6$) (b), PDGFRα and c-Met double-positive (PDGFRα⁺/c-Met⁺) ($n=3$) (c) and RIP⁺/c-Met⁺ ($n=3$) (d) cells within the field of view (FOV, 0.18 mm²; Fig. S2) of the striatum during development are shown. The results are expressed as the mean±SE. *$p<0.05$.

(green) from P3 to P14 (Figs. 4a–i). PDGFRα IR (red) also overlapped with phospho-c-Met IR (green) (Figs. 4j–l) and RIP IR (red) overlapped with phospho-c-Met IR (green) at P14 (Figs. 4m–o). Elimination of phospho-c-Met IR by pre-absorption of phospho-c-Met antibody with excess amounts of immunogen validated the specificity of the phospho-c-Met antibody (Figs. 4p–r). These findings demonstrated that c-Met, in both OPCs and oligodendrocytes, is in fact physiologically activated in the striatum during early postnatal development.

2.5. Proliferation of OPCs is promoted by intrastriatal treatment with recombinant human HGF

To determine the biological signals transduced by HGF in OPCs and oligodendrocytes, we assessed whether HGF could modulate the proliferation of OPCs and their differentiation into oligodendrocytes by stereotaxic injection of recombinant human HGF (rhHGF) into the left striatum at both P7 and P10 (0.3 or 1.0 µg per animal in each injection; Fig. 5a) and by
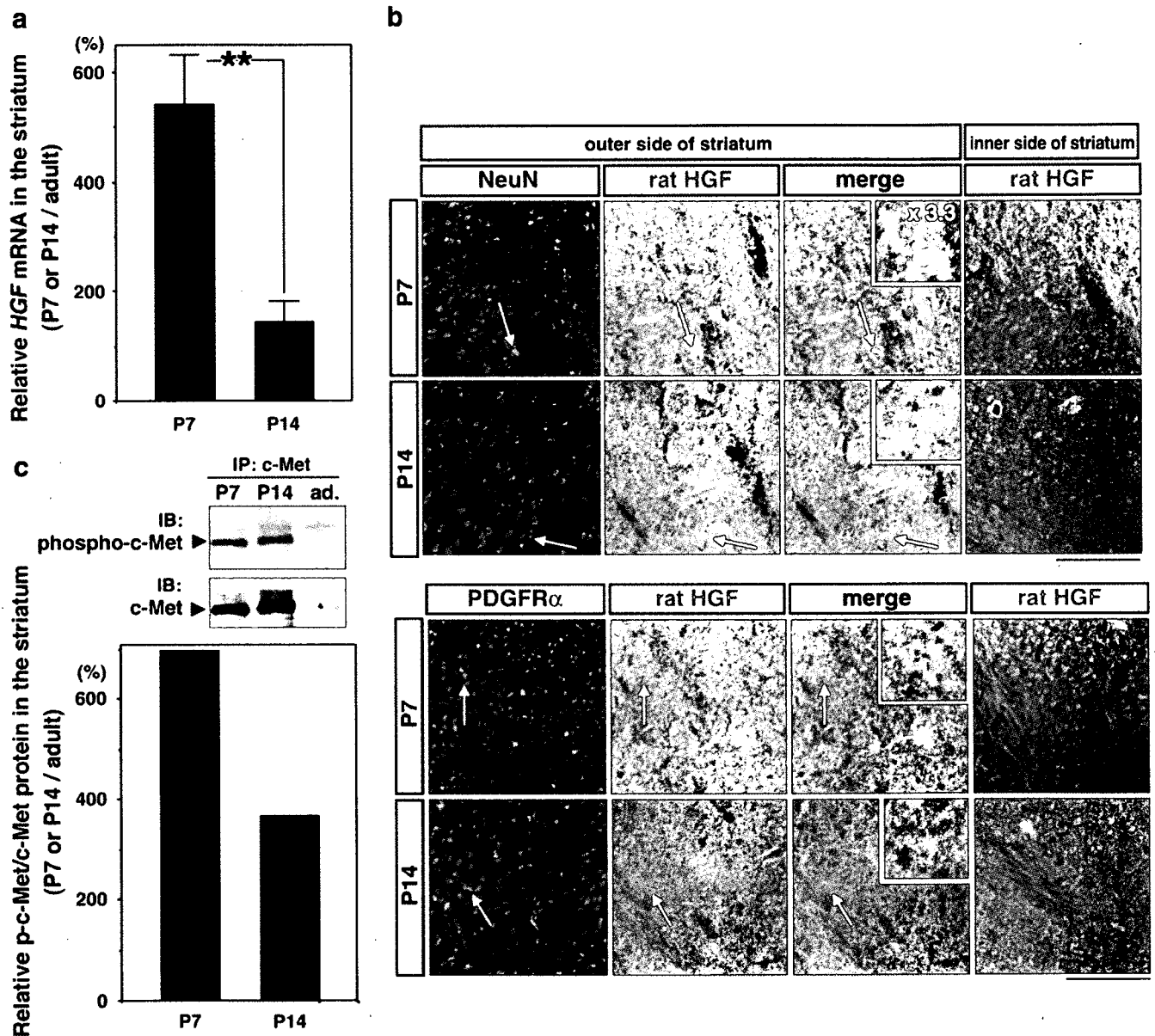
Fig. 3 – Regulation of the expression of HGF mRNA, localization of HGF IR, and phosphorylation of c-Met in the striatum during development. (a) Quantitative real-time RT-PCR of HGF in the striatum at P7 and P14 is shown (left panel). HGF mRNA levels were standardized to GAPDH mRNA. The ratio of HGF mRNA levels was expressed relative to those of adult striatum. The results are expressed as the mean ± SE. **$p < 0.01$. (b) Double fluorescence immunostaining of neuronal nuclei (NeuN) and rat HGF (right, upper) or PDGFRα and rat HGF (right, lower) in the striatum. The insets designate higher (×3.3) magnification views, indicated by white arrows. Scale bar = 100 µm. (c) Immunoprecipitation by c-Met and subsequent Western blotting of phospho-c-Met (phospho-Tyr$^{1230/1234/1235}$, p-c-Met) or c-Met during development. Lower panel shows a quantitative graph. The ratio of p-c-Met protein level per c-Met protein at P7 or P14 was expressed relative to those of adult striatum. IP, immunoprecipitation; IB, immunoblotting.

subsequent analysis of NG2⁺/BrdU⁺ cells in the striatum at P11. Two injections of PBS served as controls (Fig. 5a). Delivery of rhHGF into the striatum was confirmed in P11 rats by immunostaining using an affinity-purified antibody that was specific for human HGF and does not cross-react with rat HGF (Fig. S2). In PBS-injected control animals, substantial numbers of NG2⁺/BrdU⁺ (red/green) cells were evident, indicating the presence of large numbers of proliferating NG2⁺ OPCs at this
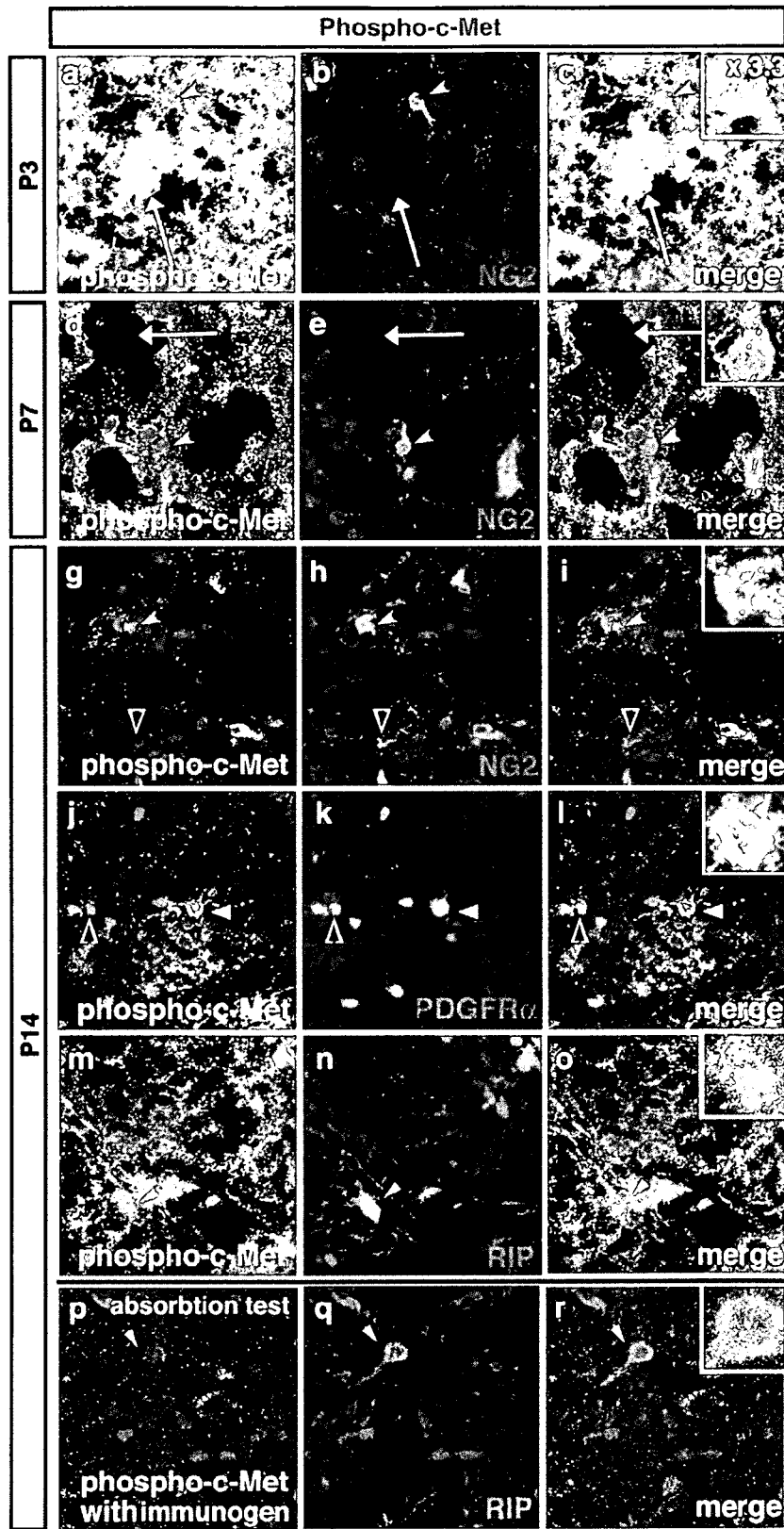
developmental stage in the striatum (Fig. 5b, upper panel, arrows). In HGF-treated animals, larger numbers of BrdU$^+$/NG2$^+$ OPCs were evident compared with controls (Fig. 5b). The relative ratio (%) of BrdU$^+$/NG2$^+$ cells per total number of NG2$^+$ cells increased to 121% and 139% by intrastriatal treatment with 0.3 μg and 1.0 μg of HGF, respectively, compared with PBS treatment (Fig. 5c, and Table 1, upper panel) as revealed by quantitative analysis in the striatum (see details in Experimental procedures; Fig. S2). These findings suggested that OPC proliferation was increased by HGF in the striatum. To further confirm the role of HGF in OPCs, we analyzed effects on the corpus callosum (white matter tissue) since larger numbers of OPCs are present in the corpus callosum compared with the striatum and phospho-c-Met IR is present physiologically in NG2$^+$ OPCs of the corpus callosum during development (Fig. 5d, e and Fig. S1). When rhHGF was injected into the striatum, we detected human HGF IR in the corpus callosum (Fig. S2). Double fluorescence immunostaining of both BrdU and NG2 revealed that the relative ratio (%) of BrdU$^+$/NG2$^+$ cells per total number of NG2$^+$ cells increased to 141% by HGF (1.0 μg) treatment compared with PBS treatment in the corpus callosum (Table 1, lower panel). Therefore, HGF promoted the proliferation of NG2$^+$ OPCs in both the striatum and corpus callosum.

2.6. The extent of OPC differentiation into MBP$^+$ oligodendrocytes is slightly diminished by HGF treatment but is slightly increased by anti-HGF IgG treatment

We next assessed whether HGF could modulate OPC differentiation into oligodendrocytes by stereotaxic injection of rhHGF into the left striatum at both P7 and P10 (0.3 or 1.0 μg per animal in each injection; Fig. 6a) and by subsequent analysis of the numbers of MBP$^+$/BrdU$^+$ cells at P11 (Fig. 6a). Two injections of PBS served as controls. In PBS-injected control animals, substantial numbers of MBP$^+$/BrdU$^+$ (red/green) cells were evident, indicating the presence of large numbers of newly formed MBP$^+$ oligodendrocytes at this developmental stage (Fig. 6b, upper panel). In HGF-treated animals, smaller numbers of BrdU$^+$/MBP$^+$ oligodendrocytes were evident compared with PBS-treated animals (Fig. 6b). The relative number of BrdU$^+$/MBP$^+$ cells decreased to 65% and 69%, by intrastriatal treatment with 0.3 μg and 1.0 μg of HGF, respectively (Fig. 6c), as revealed by quantitative analysis (see details in Experimental procedures; Fig. S2). In contrast, injection of anti-HGF "functional blocking" antibody increased the relative numbers of BrdU$^+$/MBP$^+$ cells. These findings suggest that de novo formation of oligodendrocytes was decreased by HGF but increased by anti-HGF IgG. Therefore, it seems most likely that HGF contributes to the attenuation of endogenous and exogenous differentiation of OPCs into oligodendrocytes in the striatum.

2.7. Western blot analysis of MBP reveals a reduction in MBP protein levels after treatment with HGF

To further assess the role of HGF in the modulation of MBP protein levels, Western blot analysis was performed in striatal tissues using the same injection protocol as described for Fig. 5 without BrdU (Fig. 7a). The average level of MBP protein, standardized to GAPDH protein in the striatum, decreased to 42% compared with controls after treatment with HGF (Figs. 7b, c).

2.8. HGF reduces the levels of MBP$^+$ myelin sheaths in the striatum

To determine whether the reduced levels of MBP protein in the striatum is associated with the reduced myelination of MBP$^+$ oligodendrocytes, animals were treated with either HGF or PBS using the same injection protocol as described in Fig. 7a, and the levels of MBP$^+$ myelin sheaths were quantified in the striatum at P14 (4 days after the last treatment), according to the method described by Butt and Dinsdale (2005b) with slight modification (see details in Experimental procedures). Briefly, the numbers of MBP$^+$ myelin sheaths were quantified using a grid of 20 × 20 points to yield a total of 400 points within the field of view (FOV) (3850 μm^2), and a myelin index was calculated as the percentage of points intersected by a myelin sheath. MBP IR in the HGF-treated group was lower than the PBS-treated group (Figs. 8a, b). These findings suggested that the levels of MBP$^+$ myelin sheaths decreased in the striatum after HGF treatment.

2.9. Striatal myelination is attenuated by HGF treatment

To examine the effects of HGF on myelination at the ultrastructural level, we treated animals with either rhHGF or PBS at both P7 and P10 using the same injection protocol as described in Fig. 7a. Coronal sections of the P14 rat striatum were analyzed using a HITACHI electron microscope. Fig. 9 shows representative views. In PBS-treated animals, mature myelinated axons were largely evident, while in HGF-treated animals, the numbers of myelinated axons markedly decreased. It seems unlikely that the attenuation of myelination by HGF is caused by HGF activity on neurites since immunostaining and Western blot analysis of the neurite marker, neurofilament200 (NF200), revealed that intrastriatal HGF treatment did not reduce neuritogenesis in the striatum (Figs. S3a, b). These findings suggest that HGF has an inhibitory effect on the differentiation and maturation of oligodendrocytes.
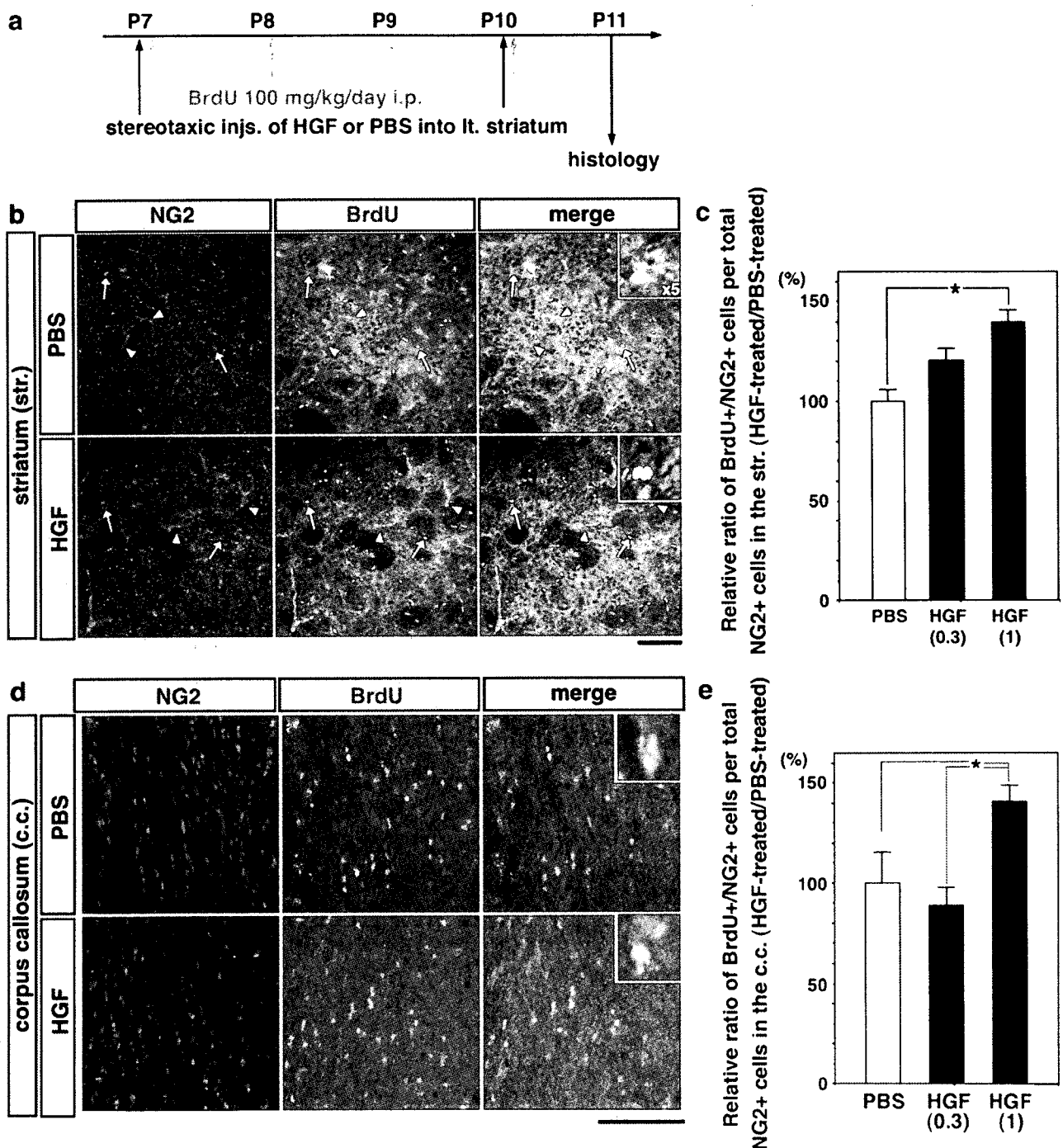
Fig. 4 – Phospho-c-Met IR is present in NG2$^+$ OPCs from P3 to P14 and in RIP$^+$ oligodendrocytes at P14. Double fluorescence immunostaining for phospho-c-Met (green) and NG2 (red) (a–i), for phospho-c-Met (green) and PDGFRα (red) (j–l), or for phospho-c-Met (green) and RIP (red) (m–o), counterstained with TOPRO-3 iodide (blue) in P3 (a–c), P7 (d–f), and P14 (g–r) rat striatum. Arrowheads indicate double-immunostained cells with NG2/phospho-c-Met (a–i), PDGFRα/phospho-c-Met (j–l), or RIP/phospho-c-Met (m–o). Bottom panel (p–r) shows the immunostaining for phospho-c-Met that is pre-absorbed with excess amounts of immunogen. Arrows indicate the positions of the bundles of innervating nerve fibers and their growth cones. The insets designate higher (×3.3) magnification views, indicated by white arrowheads. Black arrowheads indicate NG2 (red) or PDGFRα (red) single-positive cells. Scale bar = 100 μm.

3.   Discussion

Here we provided the first evidence that c-Met and tyrosine phosphorylated, and thereby activated c-Met are highly evident in both NG2+ (PDGFRα+) OPCs and RIP+ oligodendrocytes from P3 to P14 in vivo, suggesting a role for HGF in these cells. Furthermore, we also provided evidence that HGF promotes the proliferation of NG2+ OPCs in vivo by double immunohistochemical analyses of NG2+/BrdU+ cells after intrastriatal treatment with HGF at both P7 and P10, immediately after the critical point of the switch of the notch signals from Jagged1/notch/HES-1 to contactin/notch/Deltex1. This is

consistent with the previous in vitro finding that HGF promotes OPC proliferation (Yan and Rivkees, 2002), suggesting that it might result from a direct action of HGF on OPCs. In addition, we found that HGF could inhibit both the differentiation of NG2+ OPCs and the myelination of oligodendrocytes.

Although a precise molecular mechanism of this HGF effect is unclear, it has been shown that HGF has the ability to induce HES-1 mRNA production in MDA-MB-435-β4 cells and that the activation of notch leads to c-Met inhibition by the binding of HES-1 to the c-met promoter (Stella et al., 2005). Additionally, cultured bone marrow cells in the presence of HGF express both notch and Jagged1 on day 3 (Okumoto et al., 2003), suggesting a link between the HGF-c-Met signal and the notch

a   P7   P8   P9   P10   P11

BrdU 100 mg/kg/day i.p.

stereotaxic injs. of HGF or PBS into lt. striatum

histology

Table 1 – Relative values of BrdU⁺ and/or NG2⁺ cells in the striatum and corpus callosum after HGF or PBS treatment					
	PBS	HGF 0.3 µg	HGF 1 µg	HGF 0.3 µg/PBS (%)	HGF 1 µg/PBS (%)
Striatum					
BrdU⁺ cells (a)	101.7±7.0	116.8±7.0	127.0±2.6	114.9±6.9	124.9±2.6
NG2⁺ cells (b)	88.0±8.5	104.0±3.4	100.0±4.1	118.2±7.7	113.6±4.7
BrdU⁺/NG2⁺ cells (c)	26.3±3.8	37.8±2.3*	42.0±0.8*	143.4±8.5*	159.5±3.1*
Ratio of c/a (%)	26.0±2.5%	32.5±2.1%	33.5±1.3%	125.0±8.0	128.8±5.1
Ratio of c/b (%)	30.7±1.7%	37.0±1.7%	42.8±1.9%*	120.7±5.6	139.4±6.3*
Corpus Callosum					
BrdU⁺ cells (a)	45.8±4.2	52.5±2.2	57.2±7.0	114.6±4.8	124.9±15.3
NG2⁺ cells (b)	97.8±9.3	107.7±12.1	100.2±9.7	110.1±12.4	102.5±9.9
BrdU⁺/NG2⁺ cells (c)	27.8±1.6	28.7±6.2	41.7±5.9	103.2±22.3	150.0±21.2
Ratio of c/a (%)	61.1±2.1%	53.9±9.4%	72.5±2.7%	88.2±15.4	118.7±4.4
Ratio of c/b (%)	29.3±4.6%	26.0±2.6%	41.2±2.3%*	88.7±8.9	140.6±7.8*

The absolute cell number in the FOV (0.18 mm²) of P11 striatum or the FOV (0.045 mm²) of P11 corpus callosum (Fig. S2) that had been treated with PBS or HGF was expressed as mean±SE (*p<0.05).
a, the absolute number of BrdU⁺ cells in the FOV.
b, the absolute number of NG2⁺ cells in the FOV.
c, the absolute number of BrdU⁺NG2⁺ cells in the FOV.

pathway in certain types of cells. It is postulated that HGF may have the capability to induce notch signaling, presumably via a HES-1 signal in OPCs. Hence, HGF may favor proliferation of NG2⁺ OPCs but can also inhibit the differentiation of OPCs into mature oligodendrocytes even after P6.

Alternatively, it remains possible that the HGF-c-Met signals function independently of the notch signals in these processes. Colognato et al. (2004) reported a working model of the cooperation of growth factor and integrin signaling pathways. The PDGFRα-αVβ3 integrin complex induces proliferation, while axonal contact induces laminine2 binding to the α6β1 integrin complex with ErbB2/4 and, in turn, enhances survival, differentiation, and myelin formation (Colognato et al., 2004). Therefore, the modulation of such signaling pathways by HGF might be an alternative molecular mechanism. The promotion of OPC proliferation and the inhibition of its differentiation into mature myelinating oligodendrocytes may permit neurite outgrowth in the striatum at this developmental stage. The promotion of OPC differentiation into mature oligodendrocytes may lead to the presentation of myelin inhibitory proteins that inhibit axon outgrowth, such as NOGO-A/NI-220, myelin-associated glycoprotein (MAG), and oligodendrocyte-myelin glycoprotein (OMgp), on the

mature oligodendrocyte cell surface (Chen et al., 2000; McKerracher and Winton, 2002). In addition, it should be noted that NG2⁺ glial cells have been shown to provide a favorable substrate on which to grow axons (Yang et al., 2006). Indeed, this developmental stage is important for neurite outgrowth in the striatum. In the rat nigrostriatal dopaminergic system, as in all rat striatal areas where dopaminergic innervation rapidly increases from P4 to P6 (Burke, 2003; Voorn et al., 1988), higher levels of HGF mRNA might be beneficial for both OPC proliferation and inhibition of OPC differentiation to permit neurite outgrowth in a developmental stage-dependent manner. The reduction of HGF mRNA levels from P7 to P14 may permit OPC differentiation into myelinating oligodendrocytes. HGF may also play a role in differentiated oligodendrocytes; the clarification of this role is the next important issue to be examined.

In summary, we provided the first evidence that the c-Met/HGF receptor is activated in OPCs and oligodendrocytes during postnatal development and that HGF promotes the proliferation of OPCs and attenuates their differentiation into myelinating oligodendrocytes in the rat striatum. Our findings suggest a role for the HGF-c-Met system in oligodendrocyte development in concert with neuritogenesis.

Fig. 5 – NG2⁺ OPC proliferation is promoted by HGF treatment in both the striatum and corpus callosum during development. (a) The schematic illustration of the experimental protocol. Either rhHGF (0.3 or 1.0 µg per injection) or PBS was stereotaxically injected into the left striatum at both P7 and P10. BrdU (100 mg/kg) was intraperitoneally injected daily from P7 to P10. The animals were sacrificed at P11 for histological analyses. (b) Double immunostaining for NG2 and BrdU in the striatum of P11 rats that were treated with either PBS (upper panel) or rhHGF (lower panel) (1.0 µg per injection) at both P7 and P10. Arrows indicate NG2⁺ OPCs. Arrowheads indicate NG2⁺ blood vessels. Insets are the higher (×5) magnification views. Scale bar=100 µm. (c) A quantitative graph of the relative ratio of BrdU⁺/NG2⁺ cells per total number of NG2⁺ cells in the striatum. The results are expressed as the mean±SE and tested for significance with ANOVA and Scheffe's post hoc tests (*p<0.05). The average ratio of BrdU⁺/NG2⁺ cells per total number of NG2 cells in the striatum of PBS-treated rats was defined as 100%. (d) Double immunostaining for NG2 and BrdU in the corpus callosum of P11 rats that were treated with either PBS (upper panel) or rhHGF (lower panel) (1.0 µg per injection) at both P7 and P10. Scale bar=100 µm. (e) A quantitative graph of the relative ratio of BrdU⁺/NG2⁺ cells per total number of NG2⁺ cells in the corpus callosum. The results are expressed as the mean±SE and tested for significance with ANOVA and Scheffe's post hoc tests (*p<0.05). The average ratio of BrdU⁺/NG2⁺ cells per total number of NG2 cells in the corpus callosum of PBS-treated rats was defined as 100%.
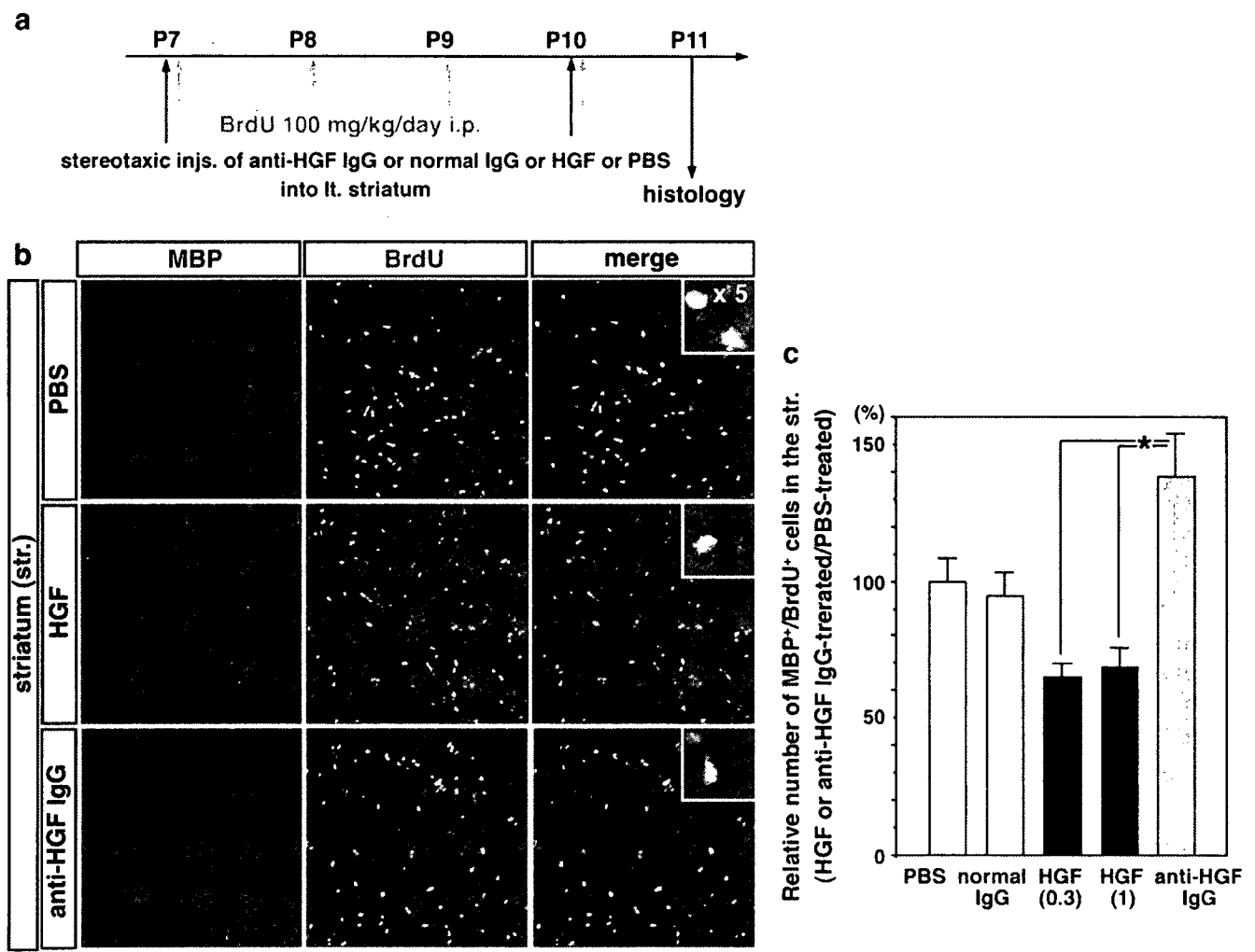
4.   Experimental procedures

4.1.   Recombinant human HGF and anti-HGF IgG

Recombinant human HGF (rhHGF) was purified from the conditioned medium of Chinese hamster ovary cells that were transfected with an expression vector containing human HGF cDNA as described earlier (Nakamura et al., 1989; Seki et al., 1990). The purity of the rhHGF was greater than 98% as determined by SDS–PAGE. Anti-rat HGF antibody was raised in rabbits after immunization of animals with recombinant rat HGF and the IgG fraction was purified using protein A-Sepharose (Pharmacia Biotech, Uppsala, Sweden), as previously described (Ohmichi et al., 1998). This anti-rat

HGF antibody does not cross-react with human HGF. One microgram of anti-rat HGF IgG neutralizes the biological activity of at least 5 ng rat HGF.

4.2.   Animals

Timed-pregnant Sprague–Dawley (SD) rats were purchased from SLC (Shizuoka, Japan) and were housed in individual cages in a temperature-controlled room under a 12-h light/12-h dark cycle. The acquisition, care, housing, use, and disposition of animals were in compliance with institutional laws and regulations of the Osaka University Graduate School of Medicine. All efforts were made to minimize animal discomfort and the number of animals used. For developmental analysis, we used SD rat pups of the following developmental time

Fig. 6 – Differentiation of OPCs into MBP+ oligodendrocytes is slightly diminished by HGF treatment and slightly increased by anti-HGF IgG treatment. (a) The schematic illustration of the experimental protocol. rhHGF (0.3 or 1.0 μg per injection), anti-HGF "functional blocking" IgG, normal IgG, or PBS was stereotaxically injected into the left striatum at both P7 and P10. BrdU (100 mg/kg) was intraperitoneally injected daily from P7 to P10. The animals were sacrificed at P11 for histological analyses. (b) Double immunostaining for MBP and BrdU in the striatum of P11 rats that were treated with PBS (upper panel), rhHGF (middle panel) (1.0 μg per injection), or anti-HGF IgG (lower panel) at both P7 and P10. Insets are the higher (×5) magnification views. Scale bar=100 μm. (c) A quantitative graph of MBP+/BrdU+ cell numbers. The results are expressed as the mean±SE and tested for significance with ANOVA and Scheffe's post hoc tests (*p<0.05). The average MBP+/BrdU+ cell number of PBS-treated rats was defined as 100%.
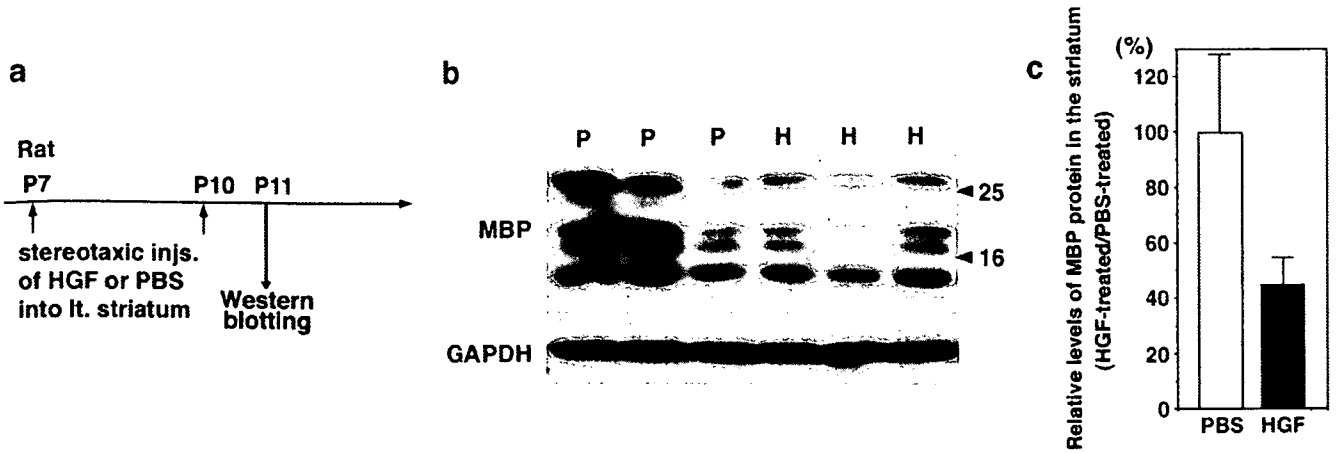
Fig. 7 – HGF reduces MBP protein levels in the striatum. (a) The schematic illustration of the experimental protocol. Either rhHGF (1.0 µg per injection) or PBS was stereotaxically injected into the left striatum at both P7 and P10. The animals were sacrificed at P11 for Western blot analysis. (b) Western blotting for MBP and GAPDH in the striatum of P11 rats that were treated with either PBS (P) or rhHGF (H). Arrowheads indicate molecular marker sizes. (c) Relative MBP protein levels were quantified and expressed as the mean±SE. The relative mean level of MBP to GAPDH proteins in the PBS-treated group was defined as 100%.

points: P3, P7, P11, P14, and postnatal week 8 (8w). To assess the role of HGF in striatal oligodendrogenesis, each SD rat that was injected with rhHGF was paired with a littermate that received injections of PBS on the same day. For injections, rats were anesthetized by intraperitoneal injection of 30 mg/kg ketamine and 5 mg/kg xylazine. The skull was placed in a stereotaxic apparatus and a 1.5-mm hole was created in the cranium. The stereotaxic coordinates for injections into the striatum were 0 mm caudal to bregma, 2.5 mm lateral to the midline, and 4.0 mm below the surface of the skull (Sherwood, 1970). Using a 30-gauge needle (Hamilton, Reno, NV) and a 10-µL Hamilton microsyringe, 0.3 µg or 1.0 µg rhHGF (1.5 or 0.5 µg/µL in PBS) (n=4 each), 10 µg anti-rat HGF IgG (5 µg/µL in PBS) (n=4), normal rabbit IgG (5 µg/µL in PBS) (n=3), or PBS (n=3) were stereotaxically injected into the striatum at 0.25 µL/min. After injection, the needle was left in place for 5 min to prevent reflux and

slowly withdrawn in several steps over 5 min. Three days after the injection (i.e., at P10), animals were re-injected with the same liquid into the same coordinates. The animals were sacrificed under deep anesthesia for both Western blotting at P11 and immunohistochemical analyses at either P11 or P14. For BrdU incorporation, BrdU (100 mg/kg, Nacalai Tesque, Kyoto, Japan) was intraperitoneally injected daily for 4 days from P7 to P10.

4.3. Tissue preparation

Animals at P3, P7, P11, or P14 were transcardially perfused with ice-cold PBS followed by ice-cold 4% paraformaldehyde (PFA) in PBS under deep anesthesia. The brains were excised and immersed in the same fixative for 1.5 h at 4 °C and the striatum was dissected prior to immunohistochemistry. Fixed
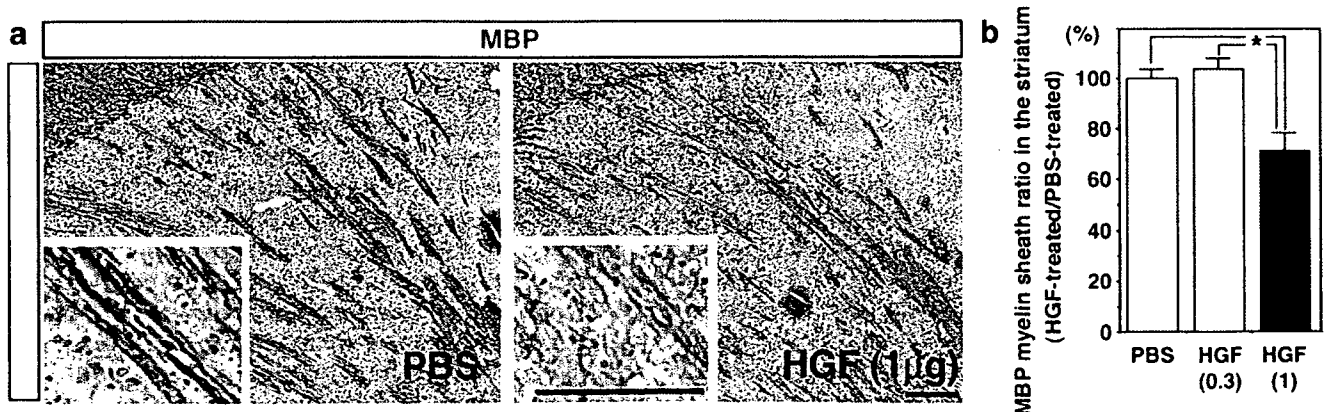
Fig. 8 – HGF reduces the number of MBP+ myelin sheaths in the striatum. (a) Immunostaining for MBP in the left striatum at P14 in animals treated with PBS (left panel) or rhHGF (right panel) (1.0 µg per injection) at both P7 and P10 using the same injection protocol described for Fig. 7a. Scale bar=100 µm. (b) The quantitative numbers of MBP+ myelin sheaths in the HGF-treated and PBS-treated striata are shown. The relative mean number of MBP+ myelin sheaths in the PBS-treated group was defined as 100%. The results are expressed as the mean±SE and tested for significance with ANOVA and Scheffe's post hoc tests (*p<0.05).
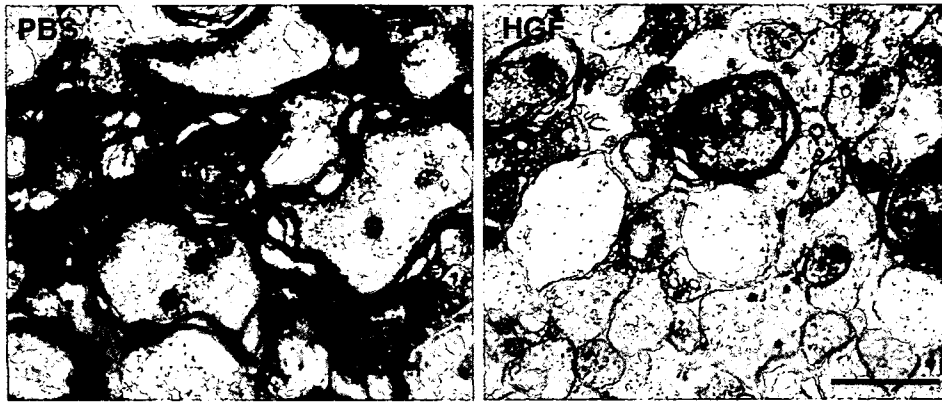
Fig. 9 – Ultrastructural examination by electron microscopy reveals the reduction of myelinated axon numbers by HGF intrastriatal treatment. Representative electron micrographs of coronal sections of the striatum at P14 in animals that were treated with either PBS (left panel) or HGF (right panel) (1.0 μg per injection) using the same injection protocol as described in Fig. 7a are shown. In the HGF-treated group, thick myelinated axons were rarely observed compared with those in the PBS-treated group. Scale bar=0.8 μm.

tissues were immersed in 20% sucrose in PBS overnight at 4 °C, frozen in CO_2, and cut into either 20-μm thick transverse or longitudinal sections using a cryostat.

4.4. Immunohistochemistry

Cryosections were incubated in blocking buffer consisting of 5% normal goat serum (S26-100 mL, CHEMICON, CA) and 0.3% Triton X-100 in PBS for 30 min at room temperature (RT) followed by one of the following primary antibodies for 1.5 h at RT: (1) rabbit polyclonal anti-c-Met antibody (1:100; sc-162, Santa Cruz, CA); (2) rabbit polyclonal anti-phospho-c-Met antibody (phospho-Tyr[1230/1234/1235], 1:100; QCB44-888, Bio-source-Invitrogen, CA); (3) rabbit polyclonal anti-MBP antibody (1:100; 01417, Stem Cell Technologies, USA); (4) mouse monoclonal anti-NG2 antibody (1:100; MAB5384, CHEMICON); (5) mouse monoclonal anti-RIP antibody (1:10000; MAB1580, CHEMICON); (6) affinity-purified rabbit polyclonal anti-human HGF antibody (1:100) (Yamada et al., 1995); (7) rabbit polyclonal anti-PDGFRα antibody (1:500, kindly provided by Dr. W.B. Stallcup); and (8) goat polyclonal anti-PDGFRα antibody (1:20, AF1062, R&D, Minneapolis). Specificity of rabbit and goat anti-PDGFRα antibodies was confirmed by double immunostaining of these antibodies as presented in Fig. S4. Immunolabeling was visualized by either fluorescence or diaminobenzidine (DAB) immunostaining. For fluorescence immunostaining, sections were incubated with secondary antibodies conjugated with either Alexa488 or Alexa546 (1:600; Invitrogen) and TOPRO-3 iodide (1:1000; Invitrogen) for nuclear staining in blocking buffer for 20 min at RT, washed with PBS, mounted with Crystal mount (Biomeda, CA), and observed under an LSM 5 PASCAL confocal microscope (ZEISS, Germany). For DAB immunostaining, sections were treated with 3% hydrogen peroxide for 5 min to quench endogenous peroxidases prior to the first antibody reaction. The sections were then incubated with primary antibody in blocking buffer for 1.5 h at RT. After washing with PBS, sections were incubated with Envision[+] System Labeled Polymer-HRP anti-mouse or anti-rabbit (Dako-Cytomation, CA) as the second antibody for 30 min at RT,

stained with DAB (0.05%), counterstained with Mayer's hematoxylin (WAKO, Japan), washed with PBS, and mounted with EUKITT (O. Kinder, Germany). The images were captured using an Olympus System Microscope BX51 (Tokyo, Japan).

4.5. BrdU incorporation

Cryosections were treated with acetone for 10 s, air-dried, washed with PBS, and incubated with 2 N HCl for 30 min at RT. After incubation with blocking buffer, sections were incubated overnight at 4 °C with rat monoclonal anti-BrdU antibody (1:100; OBT0030, Oxford Biotech. Ltd., UK), and then with either mouse monoclonal anti-NG2 antibody (1:100; MAB5384, CHEMICON) or rabbit polyclonal anti-MBP antibody (1:100; 01417, Stem Cell Technology) in blocking buffer and washed with PBS. The sections were incubated with secondary antibodies, conjugated with either Alexa488 or Alexa546 (1:600; Invitrogen), and then with TOPRO-3 iodide (1:1,000; Invitrogen) for nuclear staining. Specimens were observed under an LSM 5 PASCAL confocal microscope.

4.6. Electron microscopy

P14 rats were transcardially perfused with 2% PFA and 2% glutaraldehyde in PBS under deep anesthesia. The brains were excised and immersed in the same fixative overnight. Tissue blocks were post-fixed in 2% osmium tetroxide in PBS for 2 h at 4 °C, dehydrated through an ethanol gradient, and embedded in Epon. Ultrathin sections (90 nm) were cut with an ultramicrotome (Ultracut, Reichert-Jung) and stained with 4% uranyl acetate for 20 min at RT and with 1% Pb for 10 min at RT prior to examination by electron microscopy (H-7100, HITACHI, Japan).

4.7. Immunoprecipitation and Western blotting

Striatal lysates were prepared from the P7, P14, and 8-week-old rats in lysis buffer [50 mM Tris–HCl (pH 7.5), 150 mM NaCl, 1% Triton X-100, 10% glycerol, 25 mM β-glycerophosphate, 50 mM